CHEMISTRY
A EUROPEAN JOURNAL

Supporting Information

Fibrous Networks with Incorporated Macrocycles: A Chiral Stimuli-Responsive Supramolecular Supergelator and Its Application to Biocatalysis in Organic Media

Zhenhui Qi,[a] Changzhu Wu,[a] Paula Malo de Molina,[b] Han Sun,[c] Andrea Schulz,[a] Christian Griesinger,[c] Michael Gradzielski,[b] Rainer Haag,[a] Marion B. Ansorge-Schumacher,[b, d] and Christoph A. Schalley*[a]

chem_201300193_sm_miscellaneous_information.pdf

Table of Contents

1. General Methods.

All reagents were commercially available and used as supplied without further purification. (*R*)-(+)-α-Methylbenzyl isocyanate and (*S*)-(-)-α-methylbenzyl isocyanate were obtained from Sigma-Aldrich (ee ≥ 99 %). Lipase B from *Candida antarctica* (CalB, Lipozyme CALB L, protein content 0.24% w/w) was obtained as generous gifts from Novozymes A/S (Bagsvaerd, Denmark), purified in phosphate buffer (100 mM, pH 7.0), and lyophilized to yield a powder suitable for use. The fluorescein isothiocyanate (FITC) labeling kit was purchased from EMD Biosciences (Nottingham, UK). The tetraethyl orthosilicate (TEOS) functionalized SiO_2 nanoparticles (SiO_2@TMODS NPs*)* were prepared according to a previous report.[1] Solvents were either used as purchased or dried prior to use by usual laboratory methods. For analytical characterization of new compounds, NMR data were obtained on Bruker ECX 400 MHz, Jeol Eclipse 500 MHz, or Bruker AVANCE III 700 MHz NMR spectrometers, FTIR spectra recorded on a Nicolet Avatar 320 FT-IR spectrometer. UV/Vis spectra recorded on a Varian Cary 50 Bio UV/Vis spectrophotometer. Ultraviolet circular dichroism (CD) spectra were recorded with a Jasco J-810 spectropolarimeter at 20^{o}C. Quartz cells (1 mm path length) were used throughout. The fluorescence spectra were recorded with a PERKIN ELMER LS 50B fluorescence spectrometer.

VCD measurements. VCD spectra were measured using a Bruker VERTEX 70 spectrometer equipped with a PMA 50 side-bench module. The absorption signals were detected using a liquid-nitrogen cooled MCT infrared detector equipped with BaF_2 windows. Spectra were recorded at 4 cm^{-1} resolution. Signals were accumulated for 3,000 – 10,000 scans in about 0.5 – 2 h. The FT-IR absorbance was adjusted below 1.0 in order to attain the optimal signal-to-noise ratio in VCD measurements. A gel sample was prepared before the VCD measurements following the standard manner. The concentration of the monomer was 20.8 mM. Approximately 50 µL of the gel sample was sandwiched between two BaF_2 plates with a 50 µm spacer and a transparent film was formed between the two BaF_2 plates. The VCD was measured on a liquid cell in a standard sample holder. In order to eliminate linear dichroism effects, VCD spectra were measured by rotating the cell perpendicular to the monitoring light differently. Reproducible VCD signals were obtained.

AFM measurements. The AFM measurements have been performed using a Nanoscope Multimode V (Veeco, now Bruker AXS, Mannheim) with Nanoscope 8.10 software. The microscope was operated in the tapping mode (TM-AFM) using silicone probes NCL-W (NanoAndMore GmbH, Wetzlar) with a size of 225 µm and a tip radius of < 8 nm at resonance frequencies of 160 – 210 kHz under ambient conditions. The force constant was 31 – 71 N/m. The cantilever was forced to oscillate near its resonance frequency. The samples were prepared by spin coating (Spin Coater SCV-2) at 5.000 rpm for 20 min on freshly cleaved mica.

Rheological characterization of the gels. The native gel sample A (Figure 2) for rheological analysis was prepared as described above. Gels B – G that contained an added external stimulus were derived from these original gels by adding the stimulus, sonication at room temperature for 5 min. The aging time at room temperature was 24 hours for all gels before they were subjected to rheology. Oscillatory measurements were performed with a Malvern (Bohlin) Gemini 150 rheometer. Due to the small sample volume, a plate-plate geometry (40 mm diameter; steel) was employed at a constant temperature of 25 °C. A fixed deformation of 0.01 was used. We carefully verified during the measurements that the stress-response was always sinusoidal. No sudden jumps in the measured values were observed. Both effects would be typically observed for slip-effects so that we conclude them not to be of any significance in the measurements shown. Figure S45 (Supporting Information) shows a representative amplitude sweep confirming that the measurements were done in the linear viscoelastic regime. The measurement range was from 0.1 – 10 Hz taking 50 measurement points spaced logarithmically. The total measurement time was four minutes so that any effects of solvent evaporation are minimized.

SANS experiments. The SANS measurements were done on the KWS1 instrument of the Jülich Center for Neutron Sciences at the Forschungs-Neutronenquelle Heinz Meier-Leibnitz (JCNS at FRMII, Munich, Germany), with scattered neutrons recorded on a 128x128 3 6Li scintillation detector with CCDs detector of 68x68 cm^2. A wavelength of 4.5 Å (FWHM 10%)

and sample-to-detector distances of 1.27, 4.97 and 19.77 m were employed with collimation at 4, 8 and 20 m respectively, thereby covering a q-range of 0.026 < q < 4.5 nm^{-1}. The detector sensitivity was accounted for by comparing to the scattering of a 1 mm sample of water. Samples were measured in quartz cuvettes (QS, Hellma) of 2 mm thickness at 25°C. The fits and simulations of the SANS data were done with a model of randomly oriented homogeneous rods. For this model, the scattered intensity of a cylinder of length L, cross-section radius R and scattering contrast Δη is described by equation

$$I_{cyl}(q)={}^1N \cdot 16 \cdot (\pi \cdot R^2 \cdot L)^2 \cdot \Delta\eta^2 \cdot \int_0^1 \left(\frac{J_1\left(q \cdot R \cdot \sqrt{1-x^2}\right) \cdot \sin(q \cdot L \cdot x/2)}{q^2 \cdot R\sqrt{1-x^2} \cdot L \cdot x} \right)^2 dx + I_{inc} \qquad \text{eq. 1}$$

Where ^1N is the number density of the cylinders, J_1 is the first order Bessel function and I_{inc} the incoherent background. q is the magnitude of the scattering vector defined as:

$$q = \frac{4 \cdot \pi}{\lambda} \cdot \sin(\theta/2) \qquad \text{eq. 2}$$

with θ being the scattering angle and λ the wavelength. In order to simulate the curves in Fig. 1g we fitted the incoherent background and the forward scattering I(0) to the experimental data for several values of the cross-section radius. The length of the cylinder was taken to be large enough (L = 1000 nm) and it was verified that this choice of the length does not influence the intensity profile at the measured range of q. Basically this simply means that the length of the rods was chosen such that it was larger than our experimental observation window of several 100 nms.

2. Synthesis of New Compounds and Analytical Data

Synthesis of (*R*)-*tert*-butyl-4-((3-(1-phenylethyl)ureido)methyl)benzylcarbamate (*R*)-2. A solution of *tert*-butyl-4-(aminomethyl)benzylcarbamate (214.8 mg, 0.91 mmol) and (*R*)-(+)-α-methylbenzyl isocyanate (147 mg, 1.00 mmol) in 30 mL of CH_2Cl_2 was stirred at r.t. for 12 hours under argon atmosphere. After the reaction, the reaction mixture was poured

into diethyl ether (400 mL) and the precipitate collected, providing a white solid (55% yield). ^{1}H NMR (400 MHz, DMSO-d_6, 298 K) δ [ppm] = 1.32 (d, J = 7.0 Hz, 3H), 1.38 (s, 9H), 4.07 (d, J = 6.2 Hz, 2H), 4.14-4.16 (m, 2H), 4.75 (p, J = 6.9 Hz, 1H), 6.23 (t, J = 6.0 Hz, 1H), 6.40 (d, J = 8.1 Hz, 1H), 7.15 (br s, 4H), 7.18-7.35 (m, 5H); ^{13}C NMR (175 MHz, DMSO-d_6, 298 K) δ [ppm] = 23.34, 28.25, 42.60, 43.11, 48.67, 77.71, 125.74, 126.41, 126.82, 128.17, 138.47, 139.15, 145.77, 155.75, 157.27; ESI-TOF-HRMS: calcd. for $[M+Na]^+$ ($C_{22}H_{29}N_3O_3Na$) m/z 406.2106, found 406.2084.

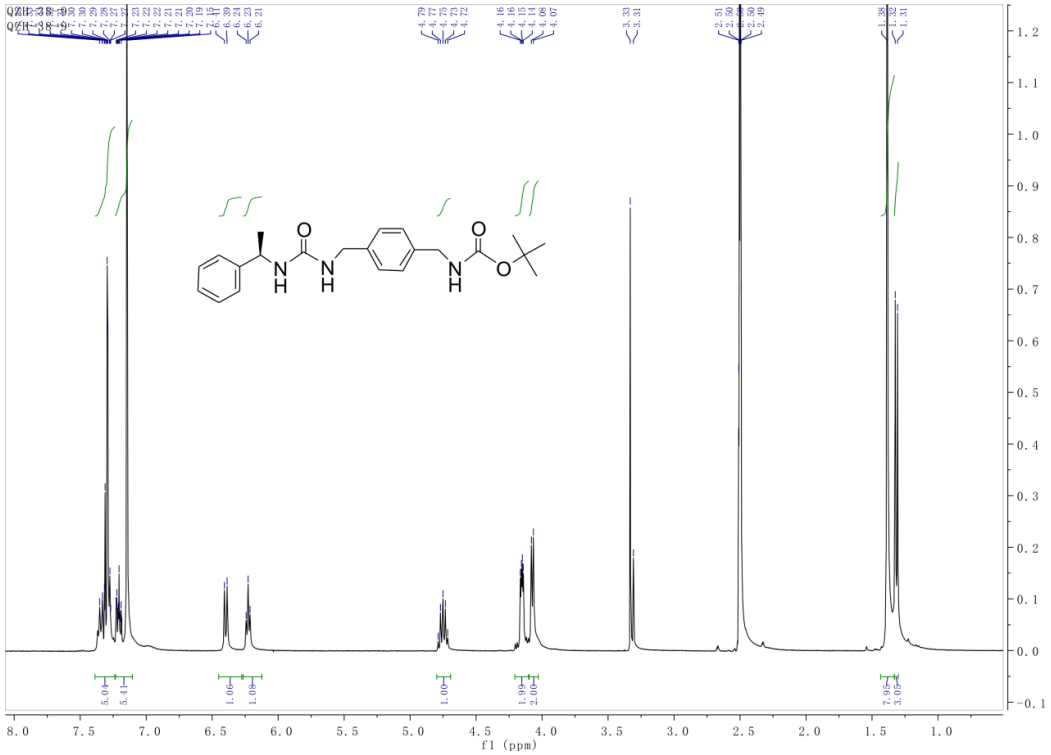

Figure S1. ^{1}H NMR spectrum (400 MHz, DMSO-d_6, 298K) of (*R*)-**2**.

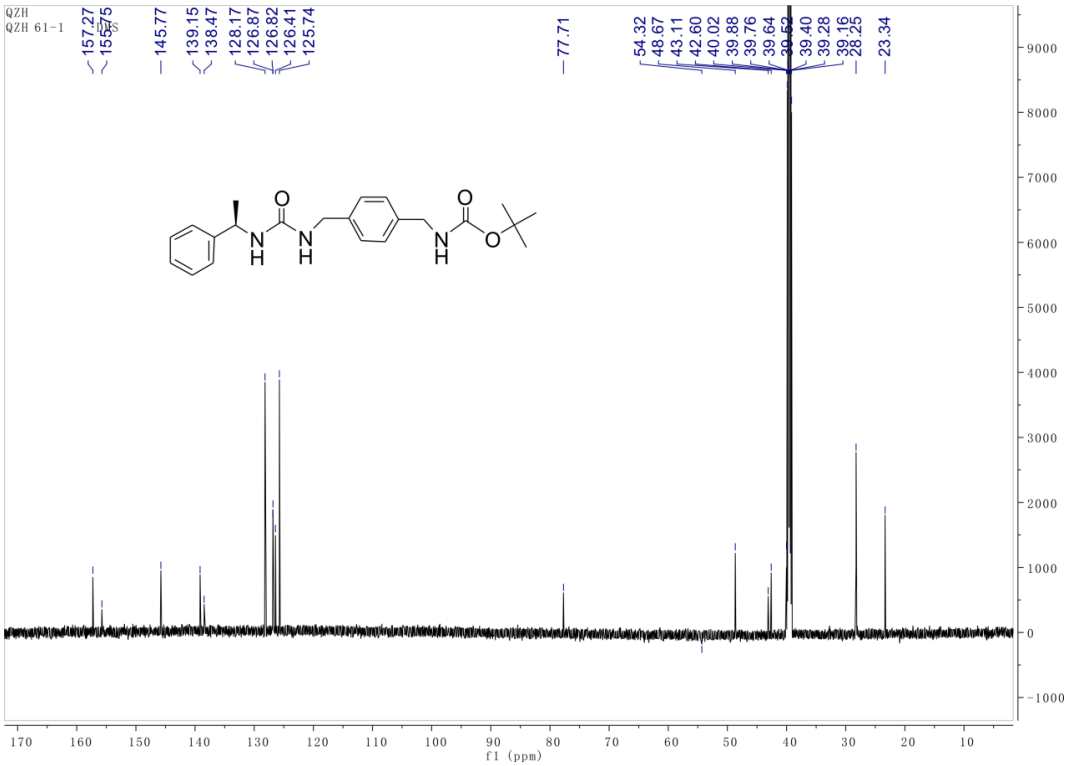

Figure S2. ^{13}C NMR spectrum (175 MHz, DMSO-d_6, 298K) of (*R*)-**2**.

Synthesis of (*S*)-*tert*-butyl-4-((3-(1-phenylethyl)ureido)methyl)benzylcarbamate (*S*)-2. (*S*)-**2** was synthesized following the procedure described above for (*R*)-**2**, using (*S*)-(-)-α-Methylbenzyl isocyanate (147 mg, 1.00 mmol). ^{1}H NMR (400 MHz, DMSO-d_6, 298 K) δ [ppm] = 1.32 (d, *J* = 7.0 Hz, 3H), 1.39 (s, 9H), 4.08 (d, *J* = 6.2 Hz, 2H), 4.15-4.17 (m, 2H), 4.76 (dq, *J* = 6.9 Hz, 1H), 6.23 (t, *J* = 6.0 Hz, 1H), 6.40 (d, *J* = 8.1 Hz, 1H), 7.15 (br s, 4H), 7.19-7.35 (m, 5H); ^{13}C NMR (175 MHz, DMSO-d_6, 298 K) δ [ppm] = 23.35, 28.25, 42.60, 43.12, 48.68, 77.71, 125.75, 126.41, 126.83, 128.18, 138.47, 139.15, 145.78, 155.75, 157.27; ESI-TOF-HRMS: calcd. for $[M+Na]^+$ ($C_{22}H_{29}N_3O_3Na$) *m/z* 406.2106, found 406.2068.

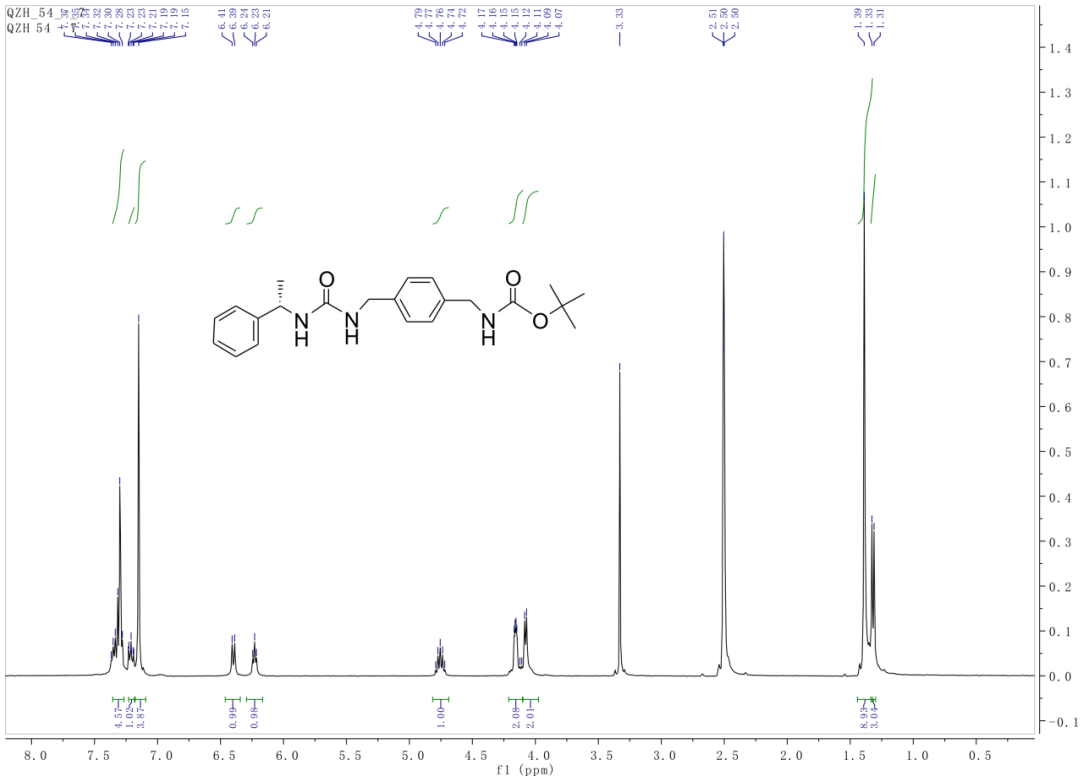

Figure S3. ^{1}H NMR spectrum (400 MHz, DMSO-d_6, 298K) of (*S*)-**2**.

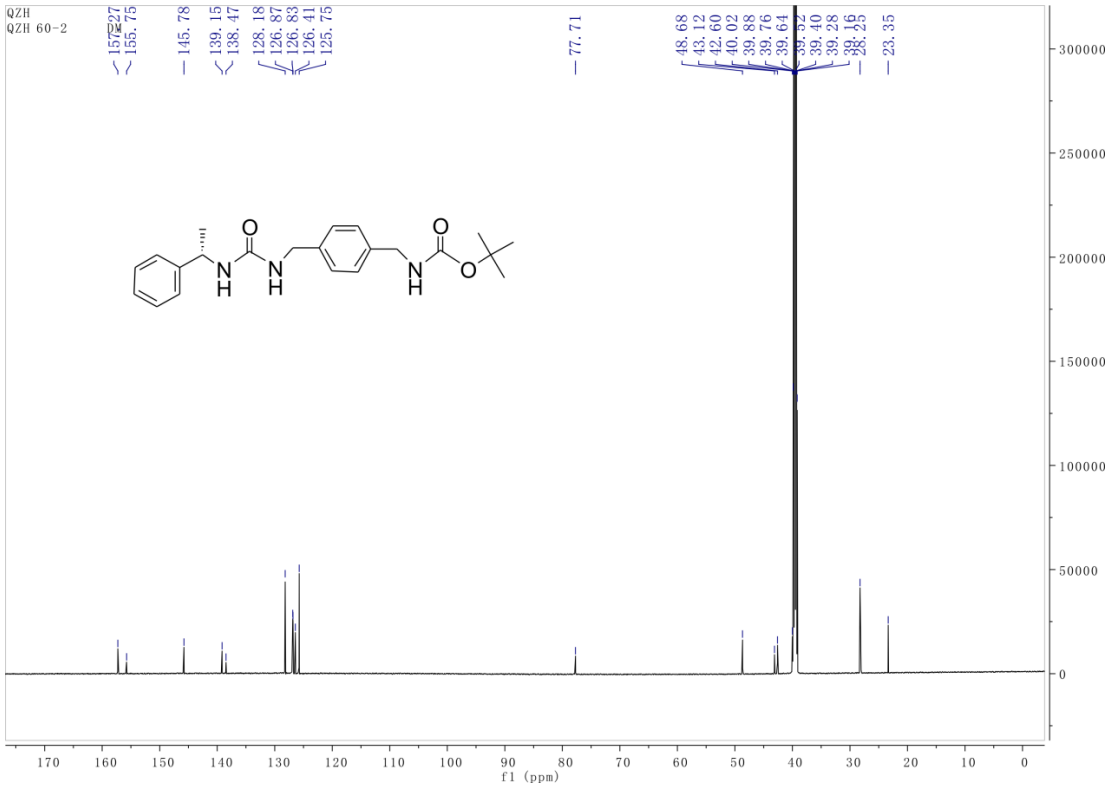

Figure S4. ^{13}C NMR spectrum (175 MHz, DMSO-d_6, 298K) of (*S*)-**2**.

Synthesis of (*R*)-1-(4-(aminomethyl)benzyl)-3-(1-phenylethyl)urea (*R*)-3. (*R*)-**2** (120 mg, 0.31 mmol) was dissolved in 10 mL of CH_2Cl_2/CH_3OH mixture (6:4 v/v) and 6 mL of trifluoroacetic acid (TFA, 78 mmol) were added. The reaction progress was monitored by TLC. After 24 h stirring at r.t., the solvent was removed in vacuo. 80 mL of 1 M aqueous sodium hydroxide solution were added to the residue and filtered to collect the precipitate. The residue was washed with small portions of water (3 x 10 mL). Then, the residue was dissolved in a CH_2Cl_2/CH_3OH mixture and filtered. The solvent was evaporated to obtain the product (91% yield). ^{1}H NMR (400 MHz, DMSO-d_6, 298 K) δ [ppm] = 1.30-1.32 (d, *J* = 8.0 Hz, 3H), 3.66 (s, 2H), 4.14-4.16 (m, 2H), 4.72-4.79 (m, 1H) 7.12-7.33 (m, 9H); ^{13}C NMR (175 MHz, DMSO-d_6, 298 K) δ [ppm] = 23.33, 42.64, 45.38, 48.64, 125.72, 126.36, 126.75, 126.83, 128.13, 138.57, 142.58, 145.78; ESI-TOF-HRMS: calcd. for $[M+H]^+$ ($C_{17}H_{22}N_3O_1$) *m/z* 284.1763, found 284.1744.

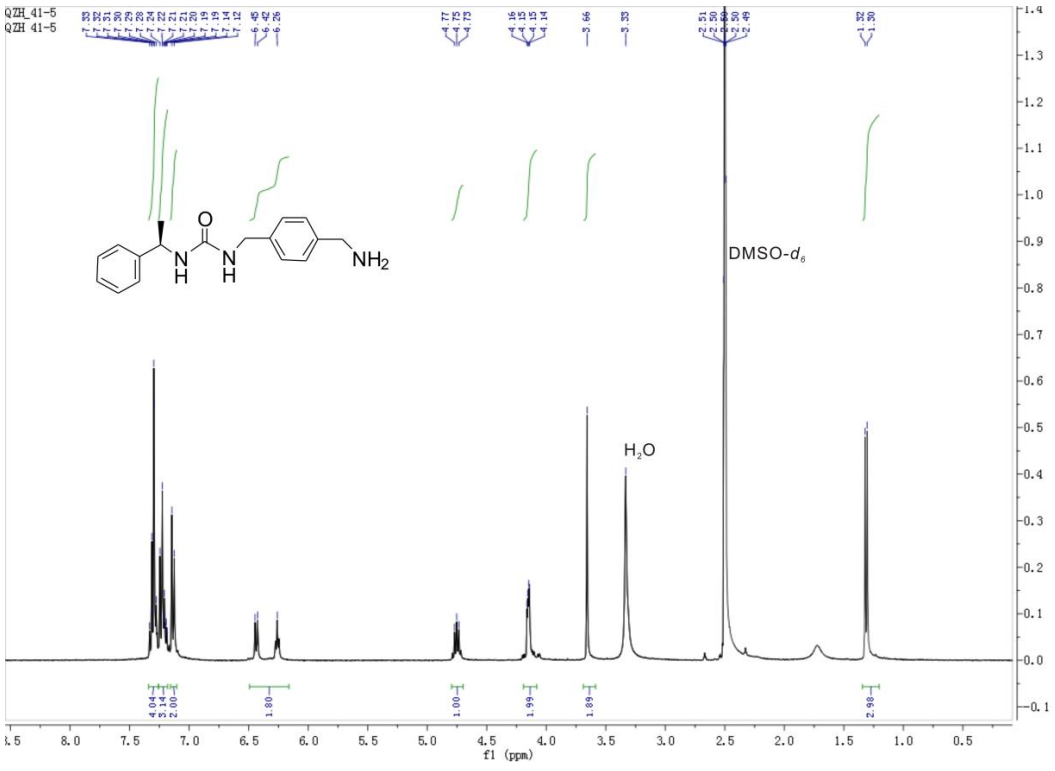

Figure S5. ^{1}H NMR spectrum (400 MHz, DMSO-d_6, 298K) of (*R*)-**3**.

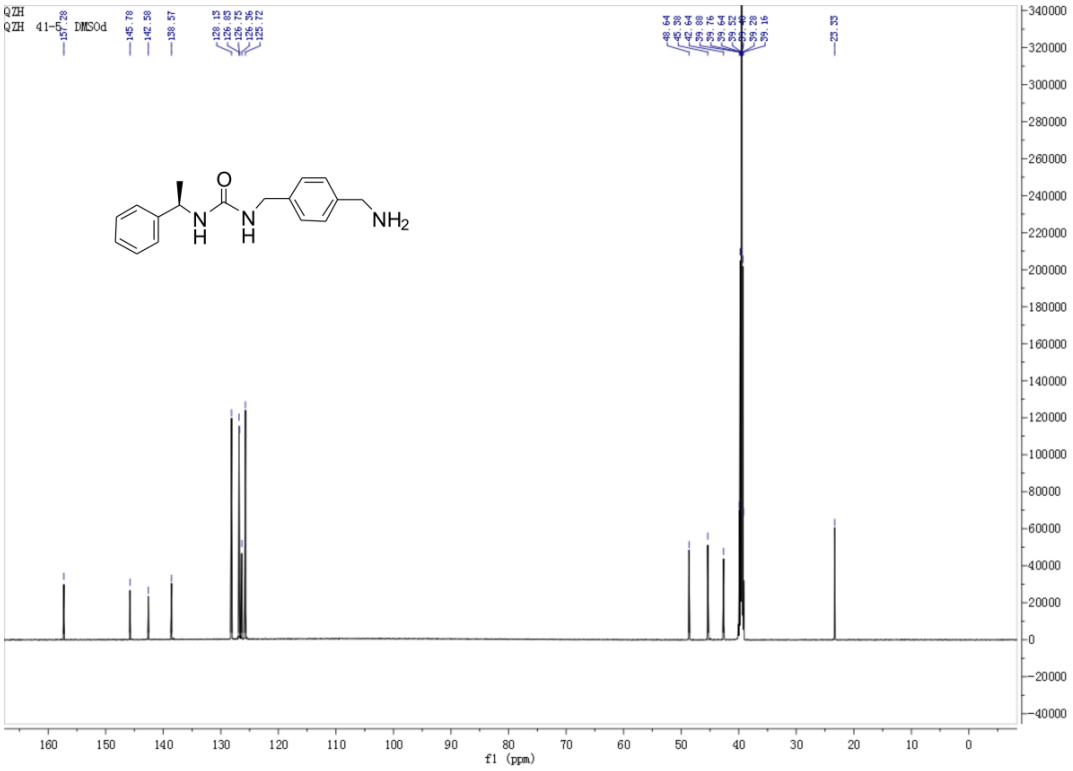

Figure S6. ^{13}C NMR spectrum (175 MHz, DMSO-d_6, 298K) of (*R*)-**3**.

Synthesis of (*S*)-1-(4-(aminomethyl)benzyl)-3-(1-phenylethyl)urea (*S*)-3. (*S*)-**3** was synthesized following the procedure described above for compound (*R*)-**3** using (*S*)-**2** as the reactant. ^{1}H NMR (400 MHz, DMSO-d_6, 298 K) δ [ppm] = 1.31-1.33 (d, *J* = 8.0 Hz, 3H), 3.67 (s, 2H), 4.16 (br. m, 2H), 4.75-4.79 (m, 1H) 7.14-7.34 (m, 9H); ^{13}C NMR (175 MHz, DMSO-d_6, 298 K) δ [ppm] = 23.34, 42.66, 45.37, 48.67, 125.74, 126.39, 126.78, 126.87, 128.16, 128.60, 142.58, 145.79, 157.32; ESI-TOF-HRMS: calcd. for $[M+H]^+$ ($C_{17}H_{22}N_3O_1$) *m*/*z* 284.1763, found 284.1764.

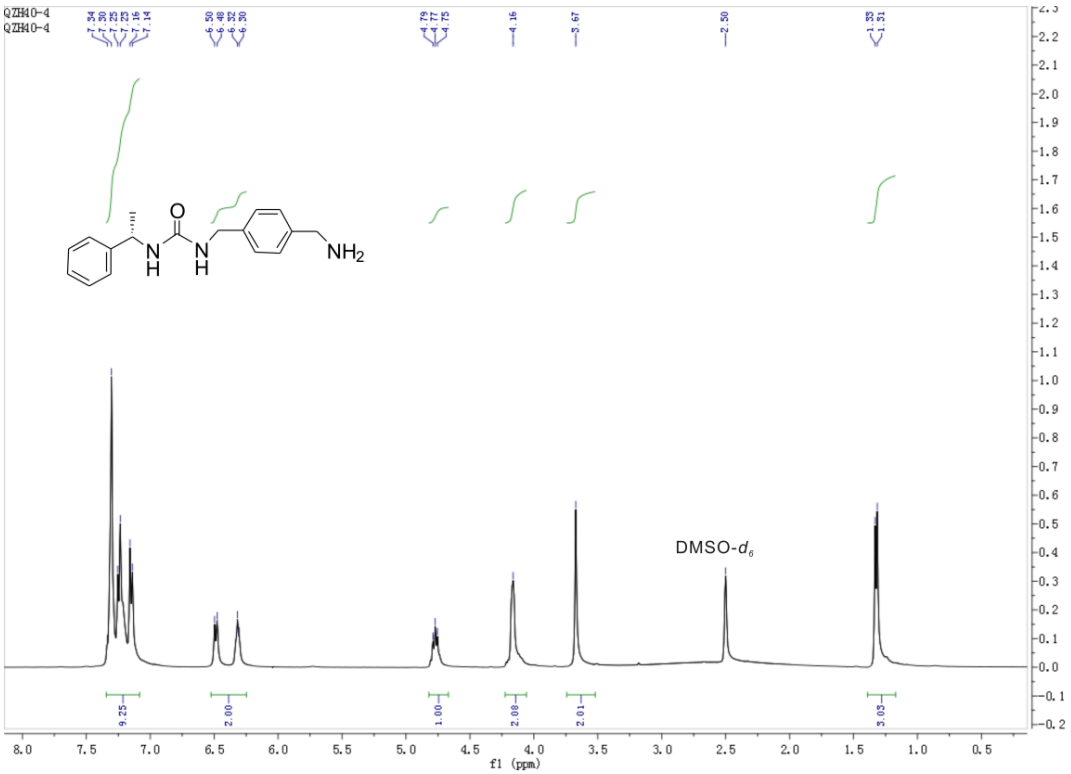

Figure S7. ^{1}H NMR spectrum (400 MHz, DMSO-d_6, 298K) of (*S*)-**3**.

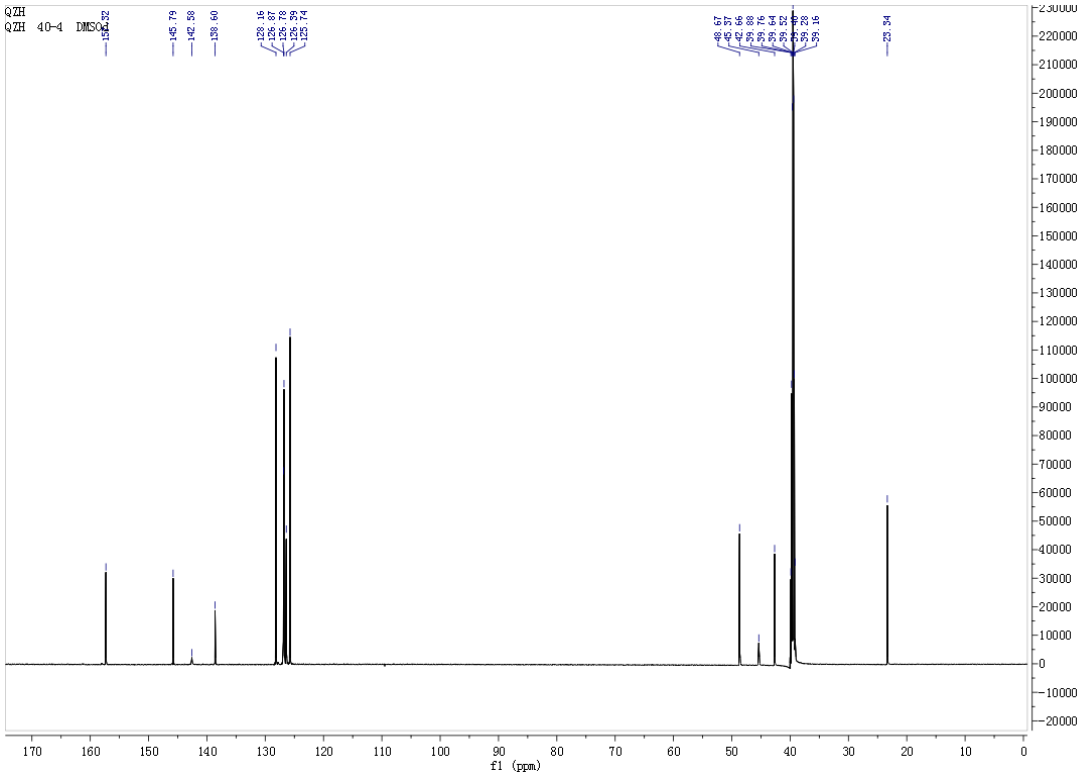

Figure S8. ^{13}C NMR spectrum (175 MHz, DMSO-d_6, 298K) of (*S*)-**3**.

Synthesis of gelator (*R*)-1. A solution of 4'-aminomethyl-benzo-21-crown-7 (**4**, 200 mg, 0.52 mmol) in dry CH_2Cl_2 (3 mL) was injected into a solution of di-*tert*-butyl tricarbonate (**5**, 134 mg, 0.52 mmol) in dry CH_2Cl_2 (6 mL) under argon atmosphere, and vigorously stirred for 40 min at r.t.. The excess of **5** was quenched by adding two drops of dry pyridine. Then compound (*R*)-**3** (116 mg, 0.43 mmol) in 3 mL chloroform was added to the isocyanate solution. The solution was vigorously stirred overnight under an argon atmosphere. After the reaction, the solvent was removed in vacuo. The residue was dissolved in 1 mL CH_2Cl_2 and then precipitated by adding 80 mL acetone. The precipitate was collected by filtration affording a pale yellow solid (60% yield). Mp: 179-180 ^{o}C. ^{1}H-NMR (500 MHz, DMSO-d_6, 298 K): δ [ppm] = 1.32 (d, *J* = 7.0 Hz, 3H), 3.53 (s, 8H), 3.55-3.57 (m, 4H), 3.59-3.61 (m, 4H), 3.72-3.76 (m, 4H), 4.02-4.06 (m, 4H), 4.13-4.20 (m, 6H), 4.76 (p, *J* = 7.0 Hz, 1H), 6.20-6.40 (m, 4H), 6.76-6.77 (m, 1H), 6.86-6.89 (m, 2H), 7.14-7.25 (m, 5H), 7.28-7.33 (m, 4H) ; ^{13}C NMR (175 MHz, DMSO-d_6, 298 K): δ [ppm] = 23.34, 42.64, 42.69, 42.71, 48.66, 68.31, 68.47, 68.97, 69.01, 69.87, 70.12, 70.19, 70.21, 112.80, 113.53, 119.41, 125.73, 126.38, 126.89, 128.15, 133.65, 139.05, 139.20, 147.76, 146.99, 148.08, 157.29, 158.04; Elemental analysis calcd (%) for $C_{37}H_{50}N_4O_9$: C, 63.96; H, 7.25; N, 8.06; Found: C, 63.97; H, 7.28; N, 8.06. ESI-TOF-HRMS: calcd for $[M+Na]^+$ $C_{37}H_{50}O_9N_4Na$, *m/z* 717.3475, found 717.3508.

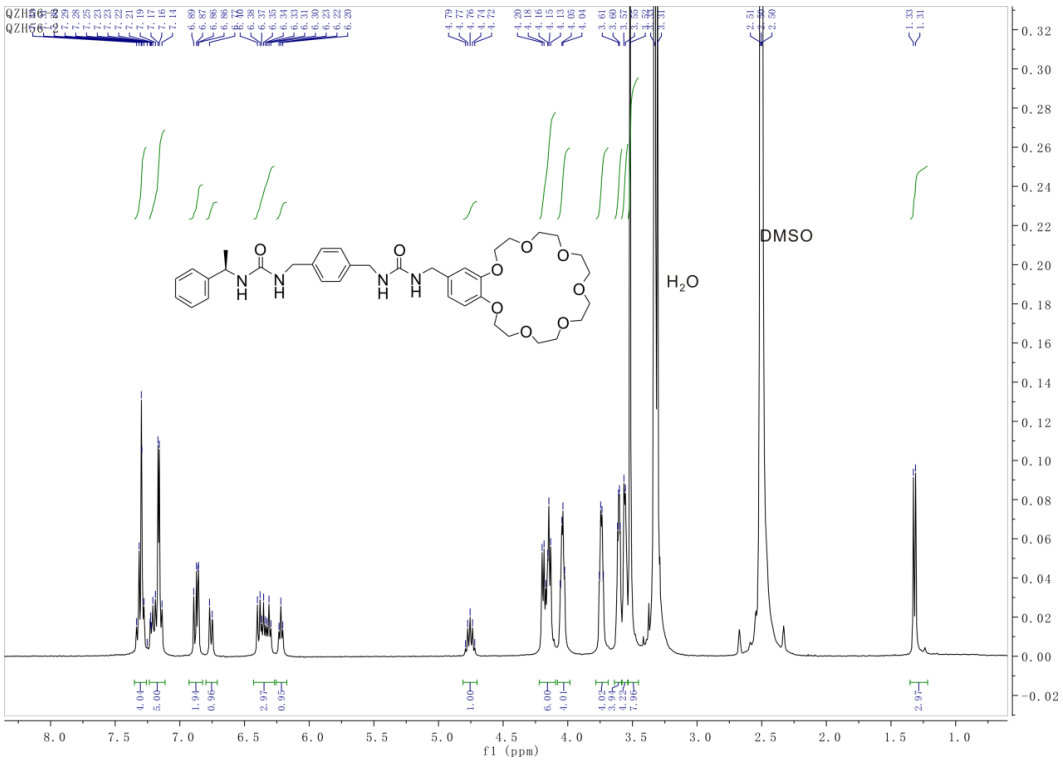

Figure S9. ^{1}H NMR spectrum (500 MHz, DMSO-d_6, 298K) of (*R*)-**1**.

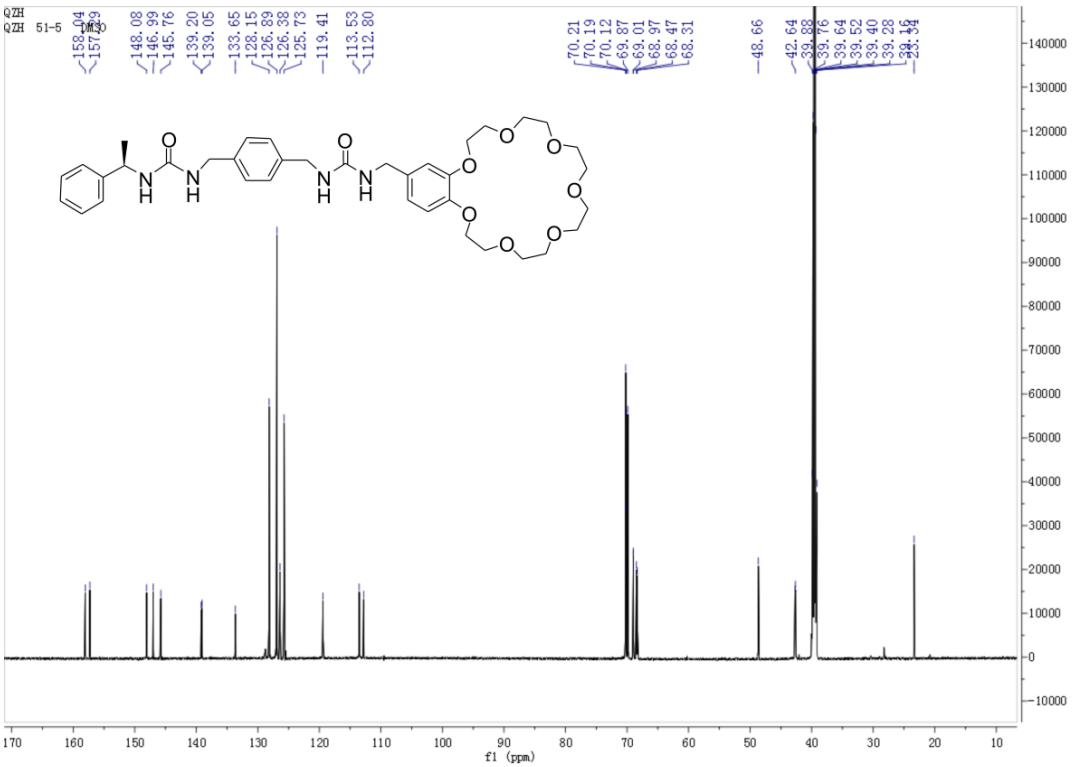

Figure S10. ^{13}C NMR spectrum (175 MHz, DMSO-d_6, 298K) of (*R*)-**1**.

Synthesis of gelator (*S*)-1. (*S*)-**1** was synthesized following the procedure described above for (*R*)-**1**, using (*S*)-**3** as the reactant. Mp: 179-180 ^{o}C. ^{1}H-NMR (700 MHz, DMSO-d_6, 298 K): δ [ppm] = 1.32 (d, *J* = 7.0 Hz, 3H), 3.53 (s, 8H), 3.56-3.57 (m, 4H), 3.61-3.63 (m, 4H), 3.74-3.76 (m, 4H), 4.04-4.06 (m, 4H), 4.14-4.20 (m, 6H), 4.77 (p, *J* = 7.1 Hz, 1H), 6.23-6.40 (m, 4H), 6.76-6.77 (m, 1H), 6.87-6.89 (m, 2H), 7.15-7.25 (m, 5H), 7.29-7.33 (m, 4H); ^{13}C NMR (175 MHz, DMSO-d_6, 298 K): δ [ppm] = 23.32, 42.62, 42.67, 42.70, 48.64, 68.31, 68.46, 68.96, 69.00, 69.87, 70.12, 70.19, 70.21, 70.22, 112.81, 113.53, 119.40, 125.71, 126.38, 126.88, 128.14, 133.63, 139.03, 139.19, 145.74, 146.98, 148.06, 157.24, 157.99; Elemental analysis calcd (%) for $C_{37}H_{50}N_4O_9$: C, 63.96; H, 7.25; N, 8.06; Found: C, 63.91; H, 7.29; N, 8.06. ESI-TOF-HRMS: calcd for $[M+Na]^+$ $C_{37}H_{50}O_9N_4Na$, *m/z* 717.3475, found 717.3474.

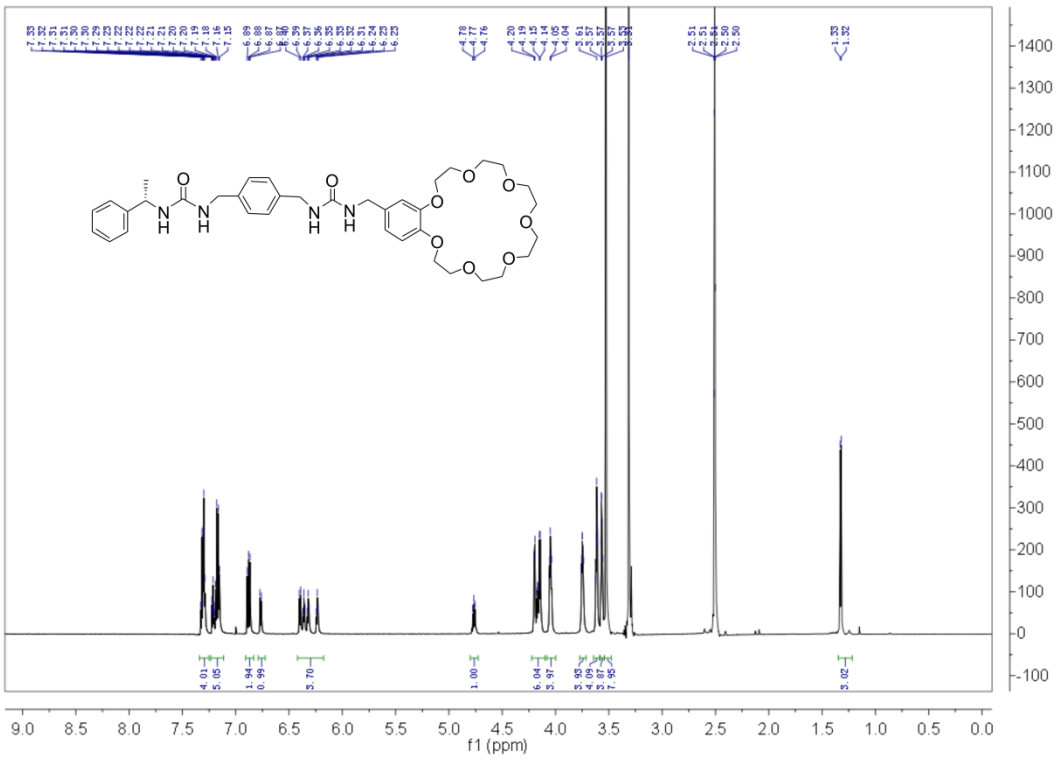

Figure S11. ^{1}H NMR spectrum (700 MHz, DMSO-d_6, 298K) of (*S*)-**1**.

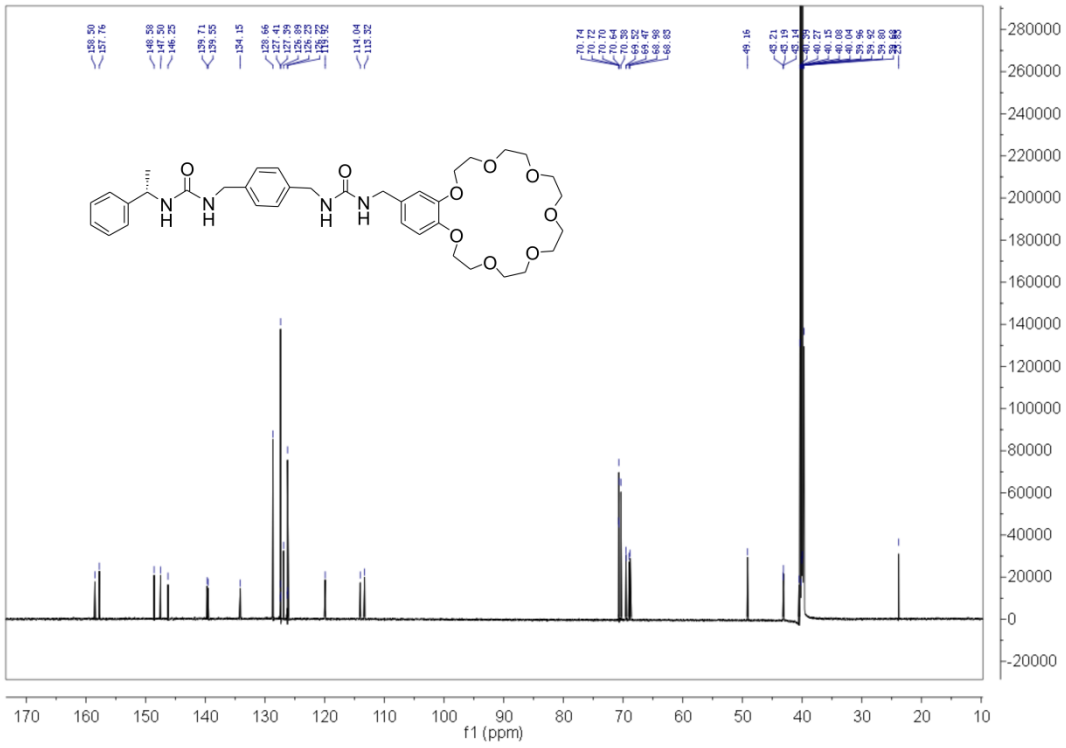

Figure S12. ^{13}C NMR spectrum (175 MHz, DMSO-d_6, 298K) of (*S*)-**1**.

3. CaChe Modeling of a Hexadecamer Core

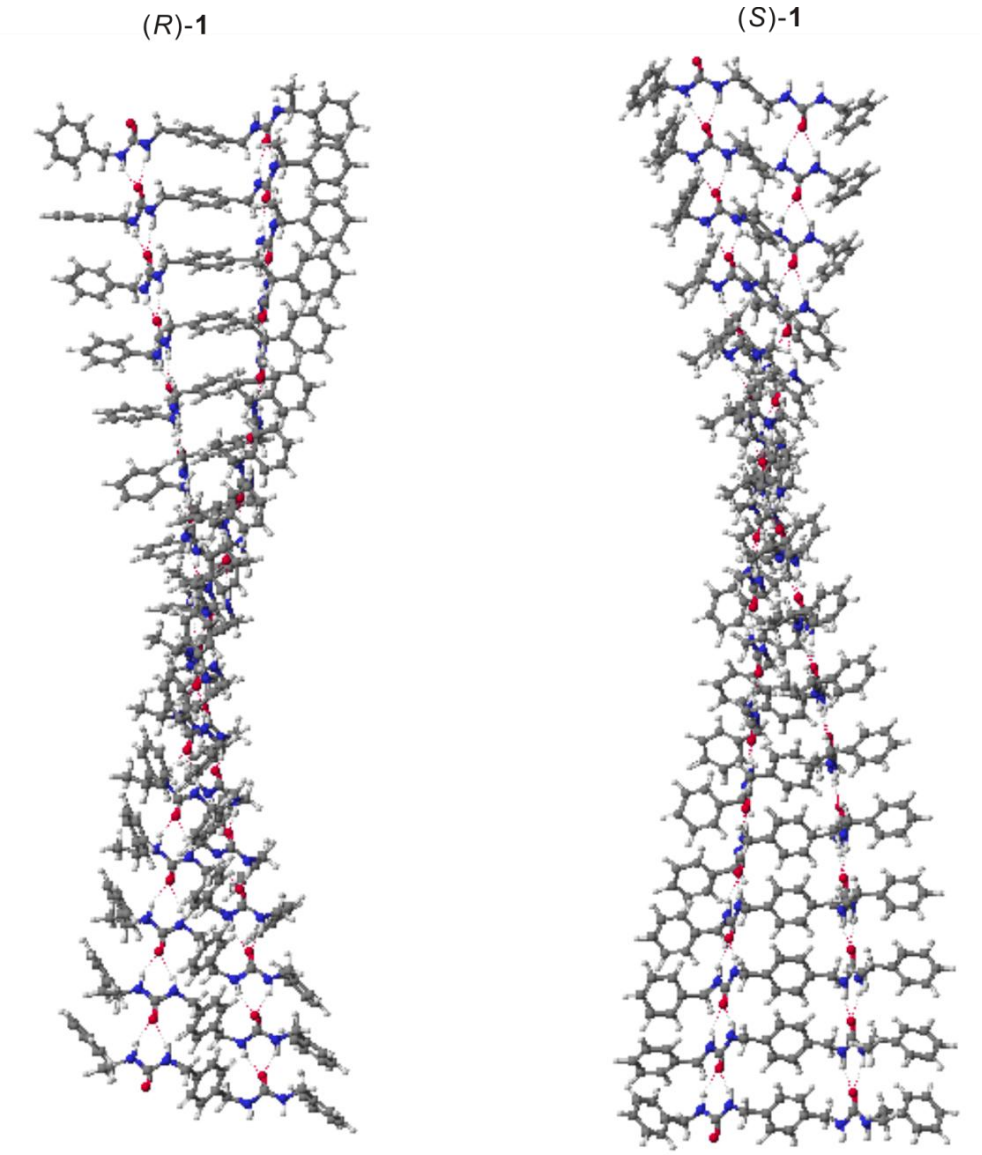

Figure S13. The core of a hexadecamer of (*R*)-**1** (left) and (*S*)-**1** (right) calculated at the AM1 MOZYME level of theory as implemented in the CaChe program package (Cache 5.0 program package, Fujitsu Inc., Krakow, Poland). Cleary, the bifurcated hydrogen bonding between the urea molecules contributes significantly to the interactions in the stacks of the gelator molecules. The crown ethers were omitted for the calculation. The calculated superstructure of the core of (*R*)-**1** adopts right-handed helicity; (*S*)-**1** left-handed helicity in agreement with experiment. Upon closer inspection, the methyl groups point sideways in these arrangements. The opposite helicity would leads to unfavorable steric interactions between the methyl groups and the next neighbor gelator molecule.

4. Characterization of the Supramolecular Gel

4.1. FT-IR Investigation of Gel (*R*)-1

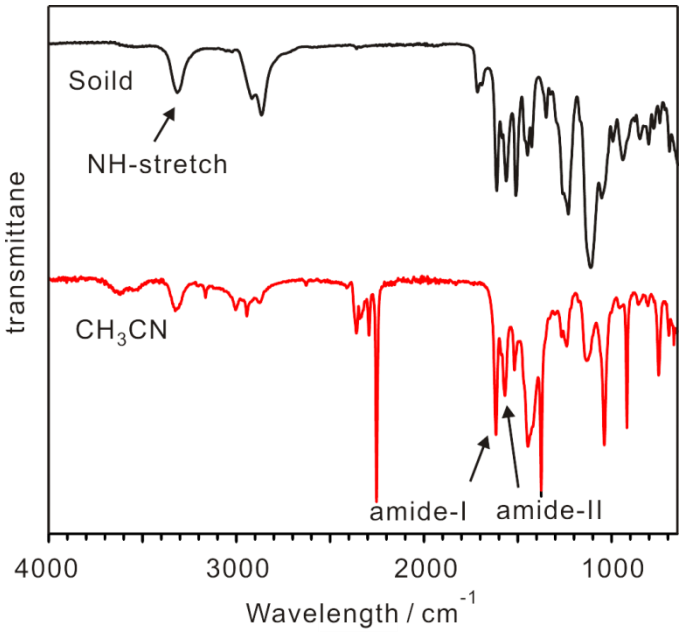

Figure S14. FT-IR spectra of (*R*)-**1** in the solid (black line) and in CH_3CN in the gel state (20.8 mM, 1.8 wt.-%, red line).

4.2. Gel-Sol Transition Temperatures T_{gs}

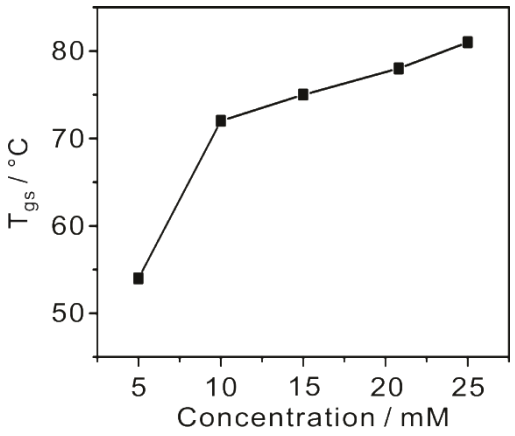

Figure S15. Plot of T_{gs} versus concentration of (*R*)-**1** in acetonitrile.

4.3. CD and LD Investigation of Gels (*R*)-1 and (*S*)-1

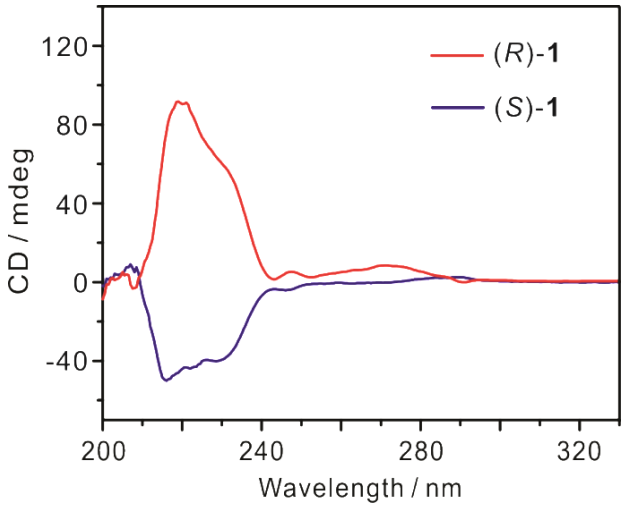

Figure S16. CD spectra of 0.127 wt.-% chiral gels in acetonitrile of: a) (*R*)-**1** (red line); b) (*S*)-**1** (blue line) at 20 °C. The CD spectra of gels recorded from (*R*)-**1** and its enantiomer of (*S*)-**1** are close to mirror images, but with some partial devation. These results point to both chiral gels to preferentially consist of fibers adopting opposite helicities. In line with AFM images, some fibers with opposite helicities are nevertheless observed, which might account for the small differences in the CD spectra.

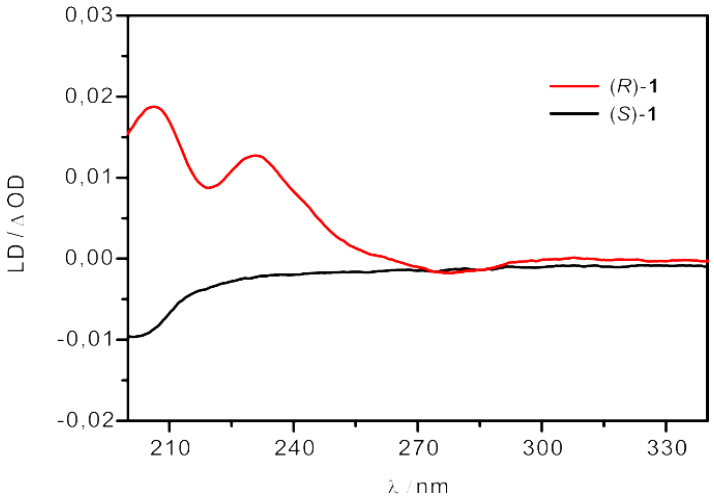

Figure S17. LD spectra of (*R*)-**1** and (*S*)-**1** measured at 25 °C under stirring (1500 rpm) in acetonitrile. The stirring direction is forward. The linear dichroism (LD) was conducted to verify the presence of LD in CD spectra. The LD value were very low and thus do not contribute significantly to the CD signals.

4.4. VCD Investigation of Gels (*R*)-1 and (*S*)-1

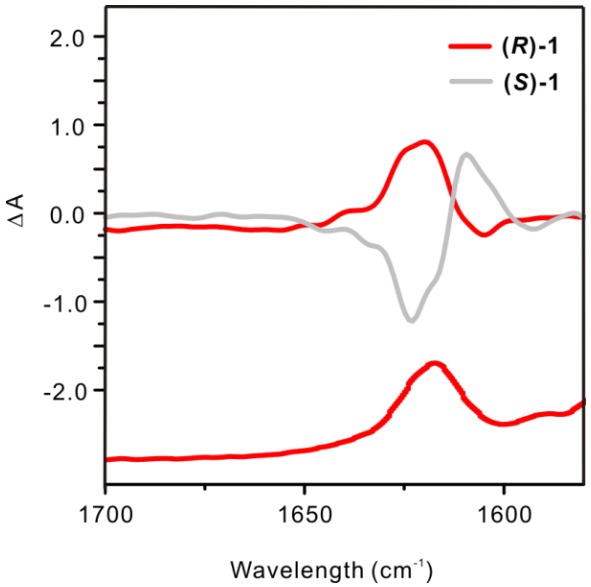

Figure S18. Observed IR (lower) and VCD (upper) spectra of chiral gels. The Figure shows the couplet peaks around 1616 cm^{-1}, which are assigned to the C=O (amide I) vibrations. The VCD spectra exhibit mirror-image relations between (*R*)-**1** and (*S*)-**1**, indicating opposite arrangement of the carbonyl groups in the helical fibers.

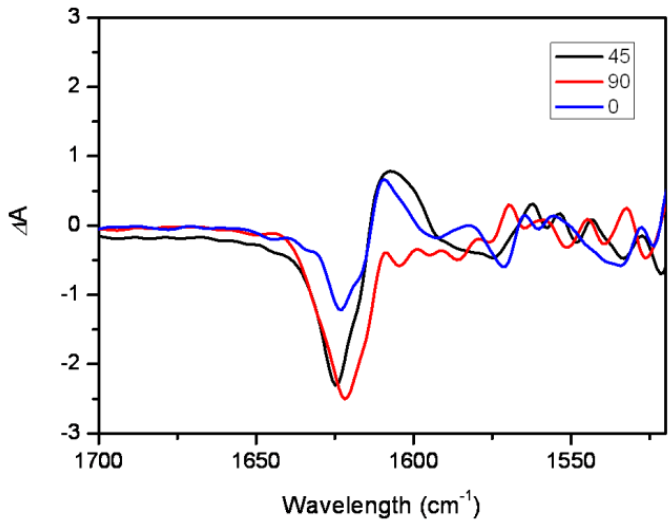

Figure S19. The observed VCD spectra of the chiral gels of (*S*)-**1**. The sample was rotated by 0, 45, and 90 deg. When the gel sample of (*S*)-**1** was rotated perpendicular to the monitoring light, no significant qualitative change of the spectra was observed thus excluding significant contributions from the linear dichroism to the VCD signals.

4.5. UV/Vis Experiments

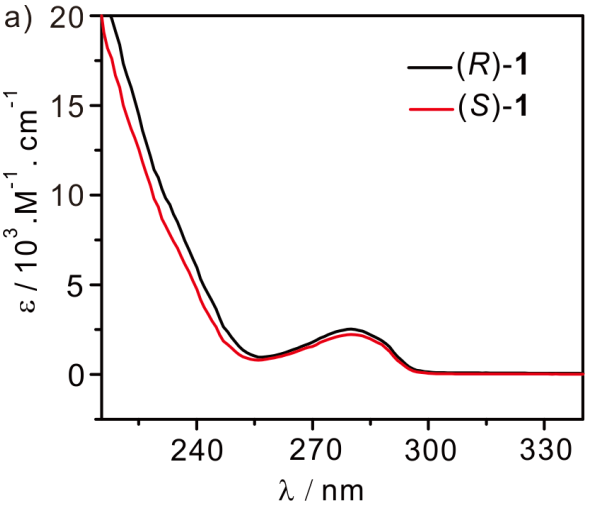

Figure S20. UV/Vis spectra of chiral gelator: (*R*)-**1** and (*S*)-**1** in acetonitrile.

4.6. Preparation of the Gel Fibers under Different Conditions

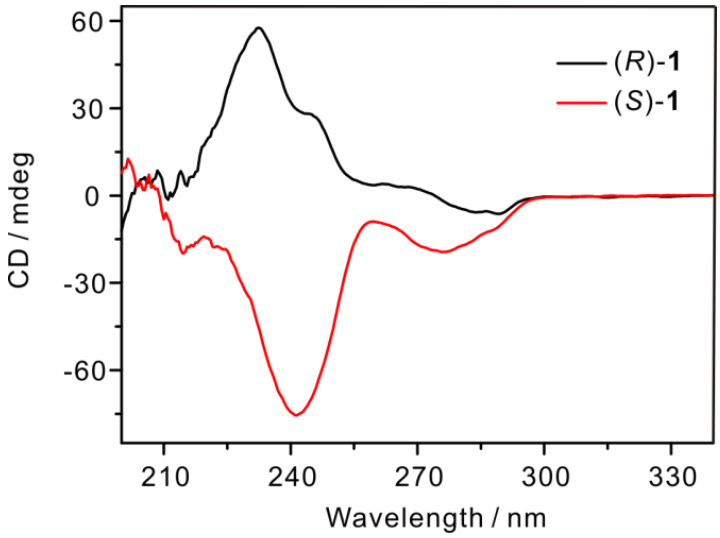

Figure S21. CD spectra of 0.44 wt.-% chiral gels in acetonitrile of: a) (*R*)-**1** (black line); b) (*S*)-**1** (red line) at 20 °C. These samples were prepared and heated at 75 °C for 30 min, and then cooled immediately to room temperature without further annealing.

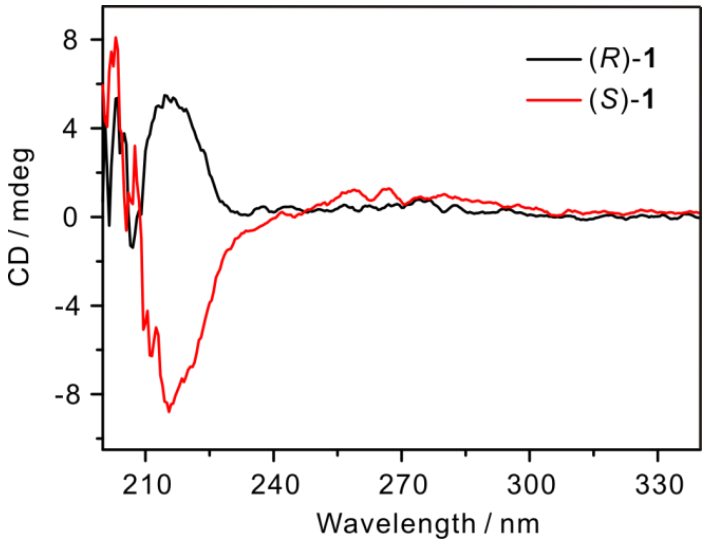

Figure S22. CD spectra of 0.44 wt.-% chiral gels in acetonitrile of: a) (*R*)-**1** (black line); b) (*S*)-**1** (red line) at 20 °C. These samples were prepared and heated at 75 °C for 30 min, then followed by annealing process. The annealing process was achieved by keeping the sample vials in the oil bath which was slowly cooled from 75 °C to room temperature.

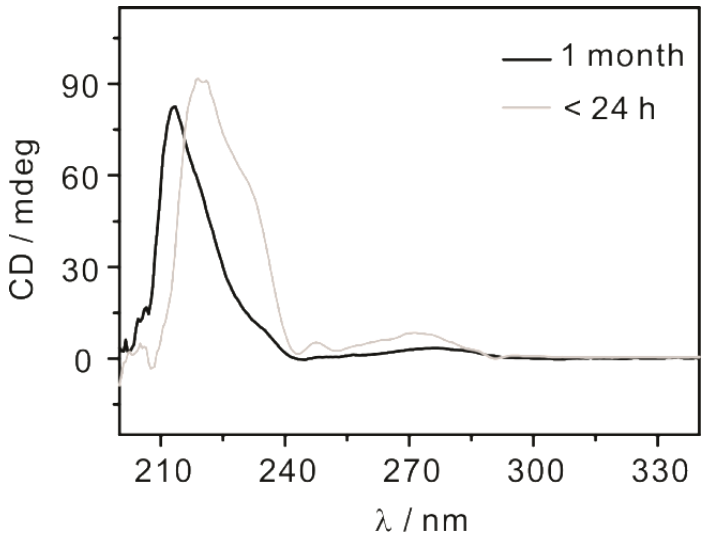

Figure S23. CD spectra of (*R*)-**1**(0.127 wt.-%) in acetonitrile recorded a) 24 h after mixing (black line); b) over a period of 1 month at 20 °C. The time-dependent experiment of (*R*)-**1** revealed a minor change in the peak shape, but not the amplitude, indicating a slow ageing process of the fibrous structures.

4.7. Morphology Investigation of (*R*)-1 and (*S*)-1 by AFM

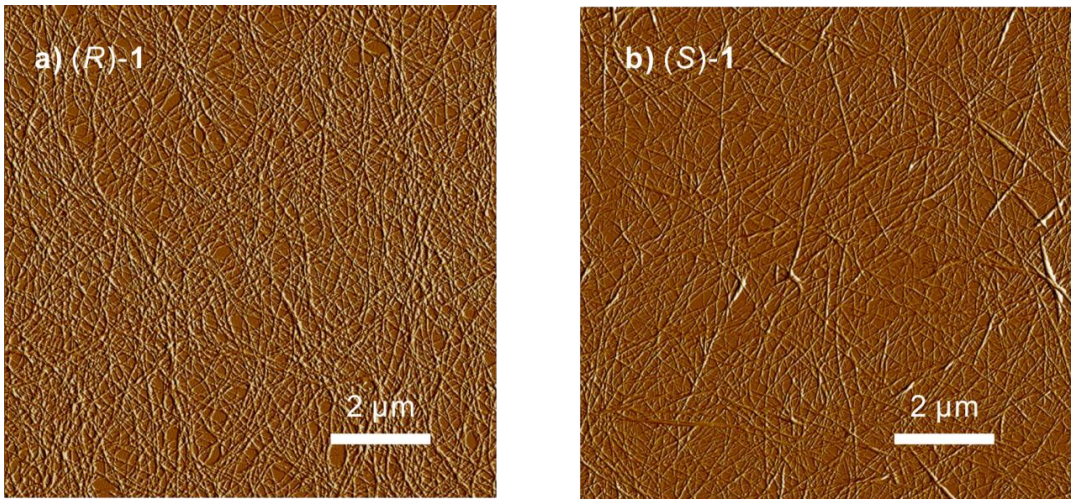

Figure S24. The morphology of a) (R)-1 and b) (S)-1 on mica as observed by AFM: The samples were diluted from high concentration (0.127 wt.-% in acetonitrile) to 0.02 wt.-% directly before spin-coating. Highly entangled fibers still dominate in the images.

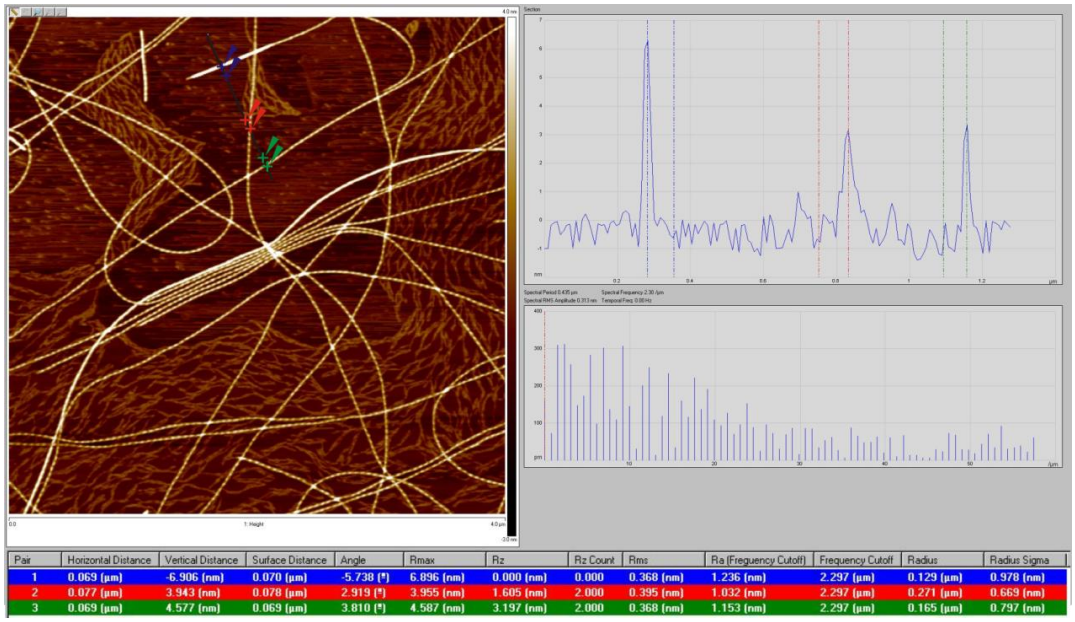

Figure S25. A height profile providing evidence for the co-existence of bundled fibers (6.9 nm high) and single fibrils (3.9 nm high) in the AFM image of (*S*)-**1**. The fibers thus have almost twice the height of the fibrils, suggesting fibrils that tend to wind around each other to form bundles of either two or four fibrils. Height measurements were done between the highest part of each helix turn and the blank surface next to the fibers

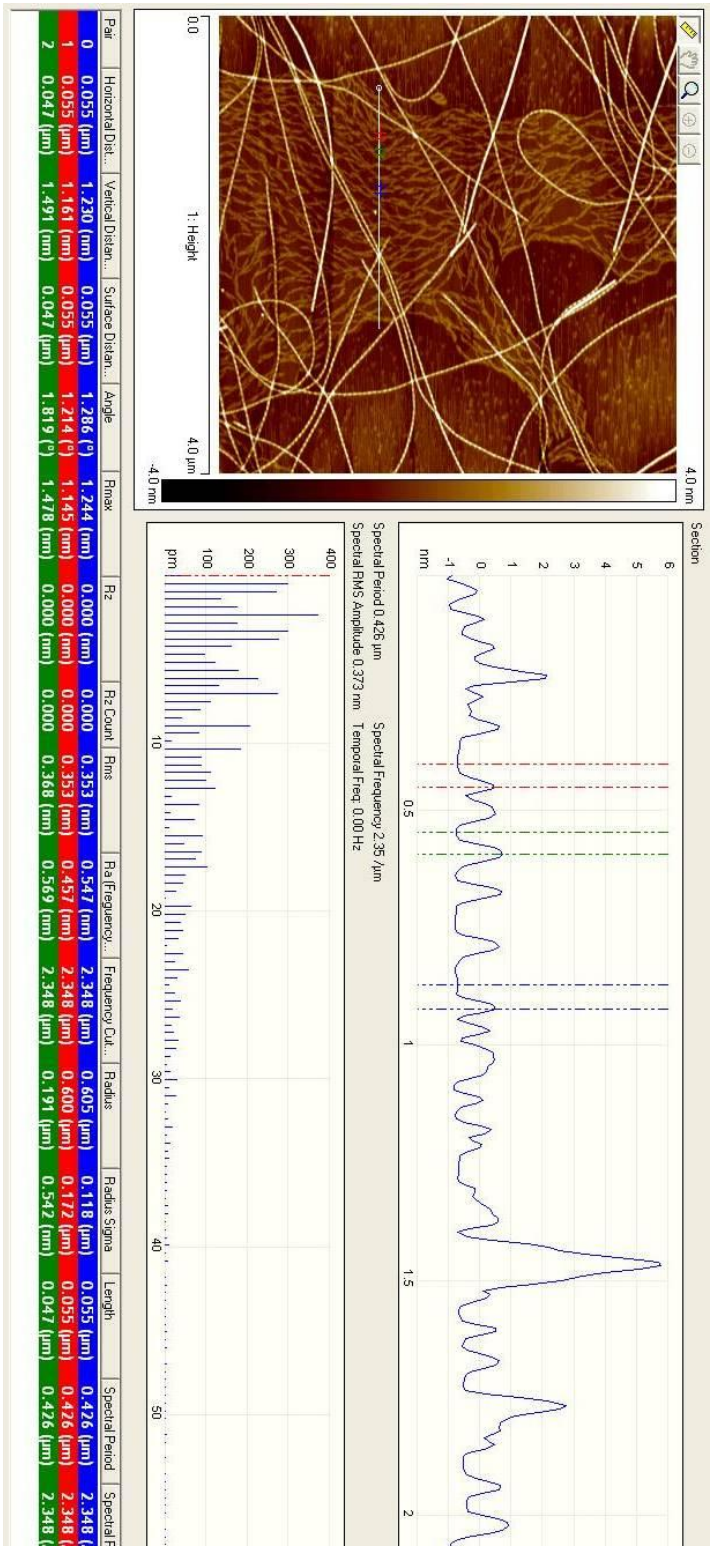

Pair	Horizontal Dist...	Vertical Distan...	Surface Distan...	Angle	Rmax	Rz	Rz Count	Rms	Ra (Frequency...	Frequency Cut...	Radius	Radius Sigma	Length	Spectral Period	Spectral F
0	0.055 (µm)	1.230 (nm)	0.055 (µm)	1.286 (°)	1.244 (nm)	0.000 (nm)	0.000	0.353 (nm)	0.547 (nm)	2.348 (µm)	0.605 (µm)	0.118 (µm)	0.055 (µm)	0.426 (µm)	2.348 (
1	0.055 (µm)	1.161 (nm)	0.055 (µm)	1.214 (°)	1.145 (nm)	0.000 (nm)	0.000	0.353 (nm)	0.457 (nm)	2.348 (µm)	0.600 (µm)	0.172 (µm)	0.055 (µm)	0.426 (µm)	2.348 (
2	0.047 (µm)	1.491 (nm)	0.047 (µm)	1.819 (°)	1.478 (nm)	0.000 (nm)	0.000	0.368 (nm)	0.569 (nm)	2.348 (µm)	0.191 (µm)	0.542 (nm)	0.047 (µm)	0.426 (µm)	2.348 (

Figure S26. The height profile showing the height f small unknown fibrous like objects is around 1.2 nm.

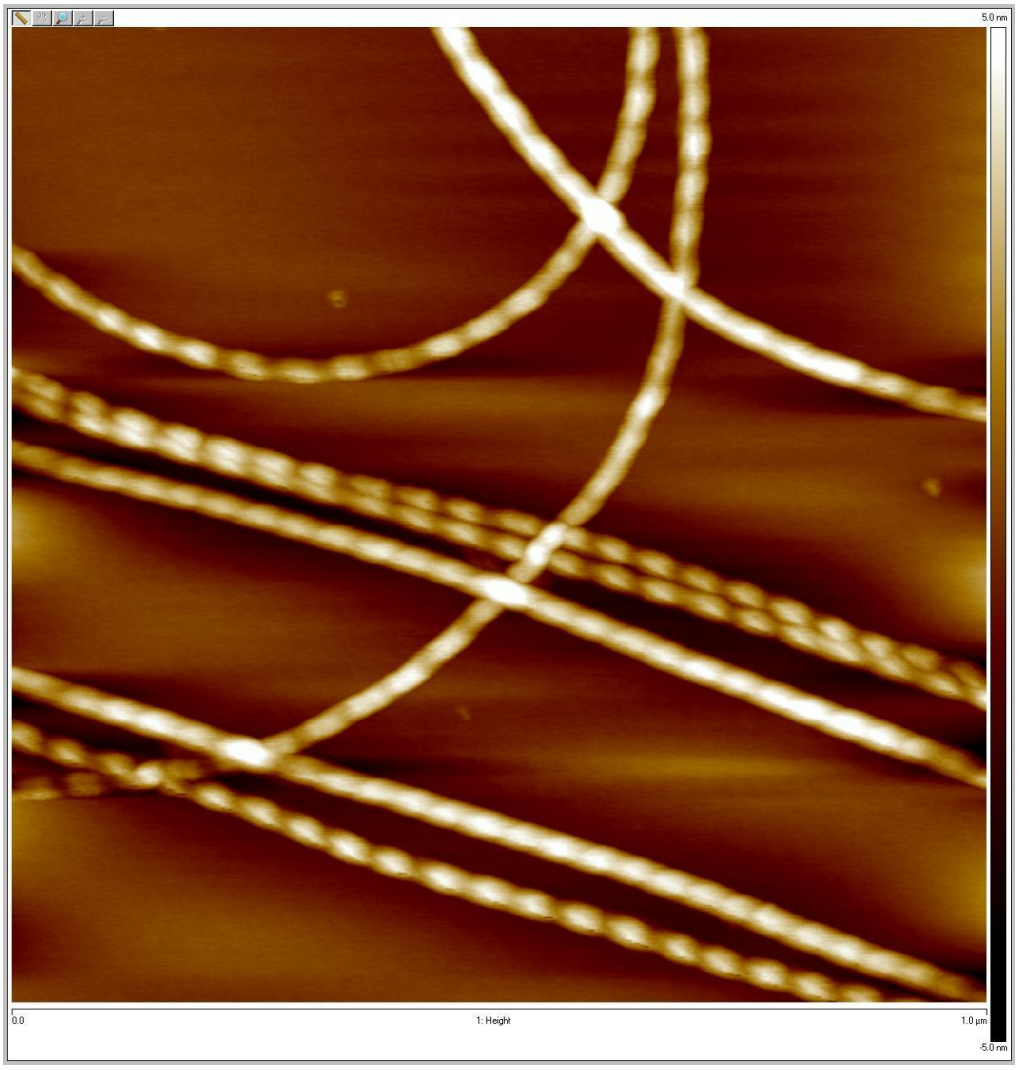

Figure S27. AFM height image of sample (*R*)-**1** prepared by spin-coating of solution obtained by dilution of 0.127 wt-% chiral gels in acetonitrile to 0.05 wt-%.

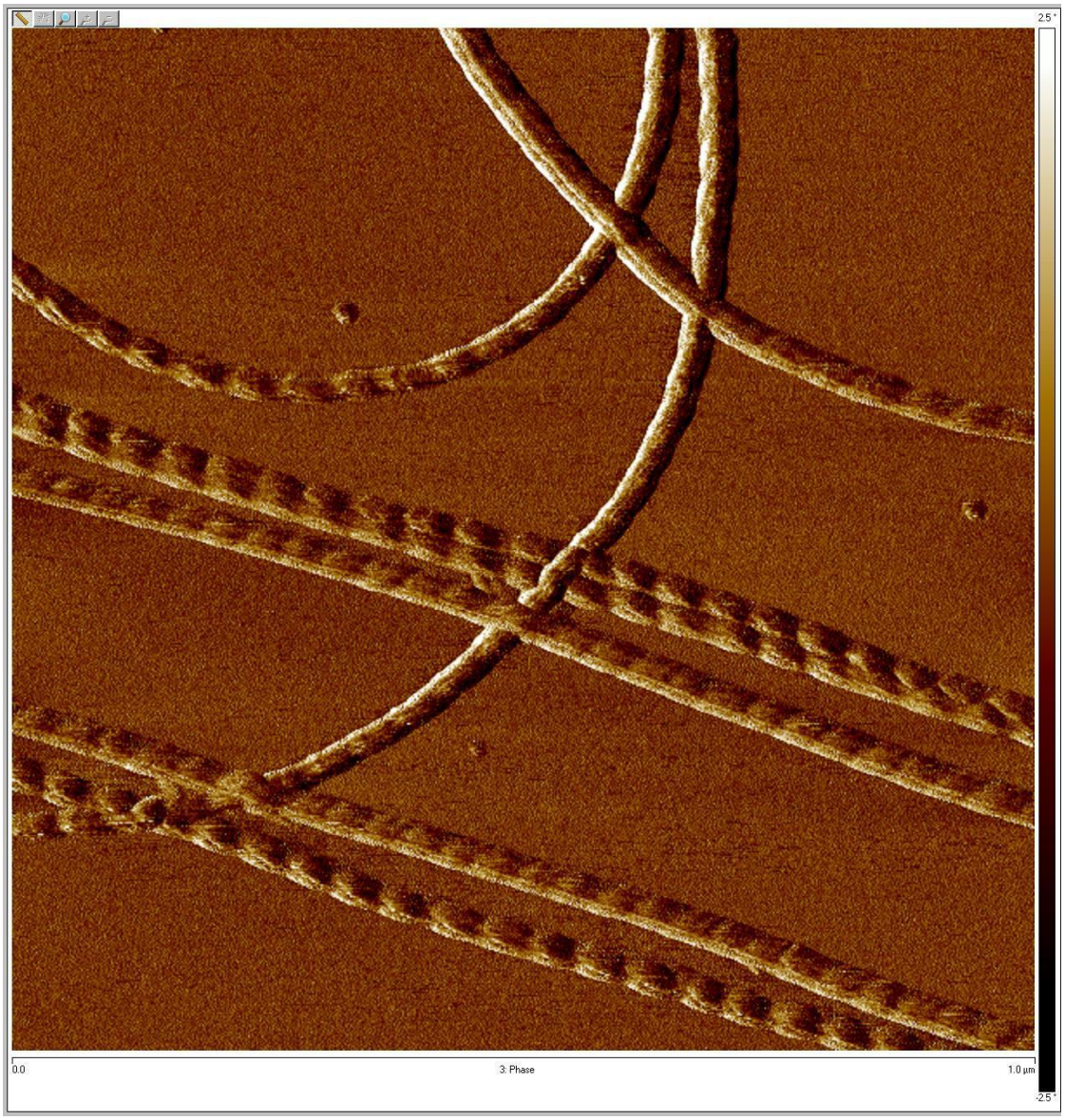

Figure S28. AFM phase image of sample (*R*)-**1** prepared by spin-coating of solution obtained by dilution of 0.127 wt-% chiral gels in acetonitrile to 0.05 wt-%.

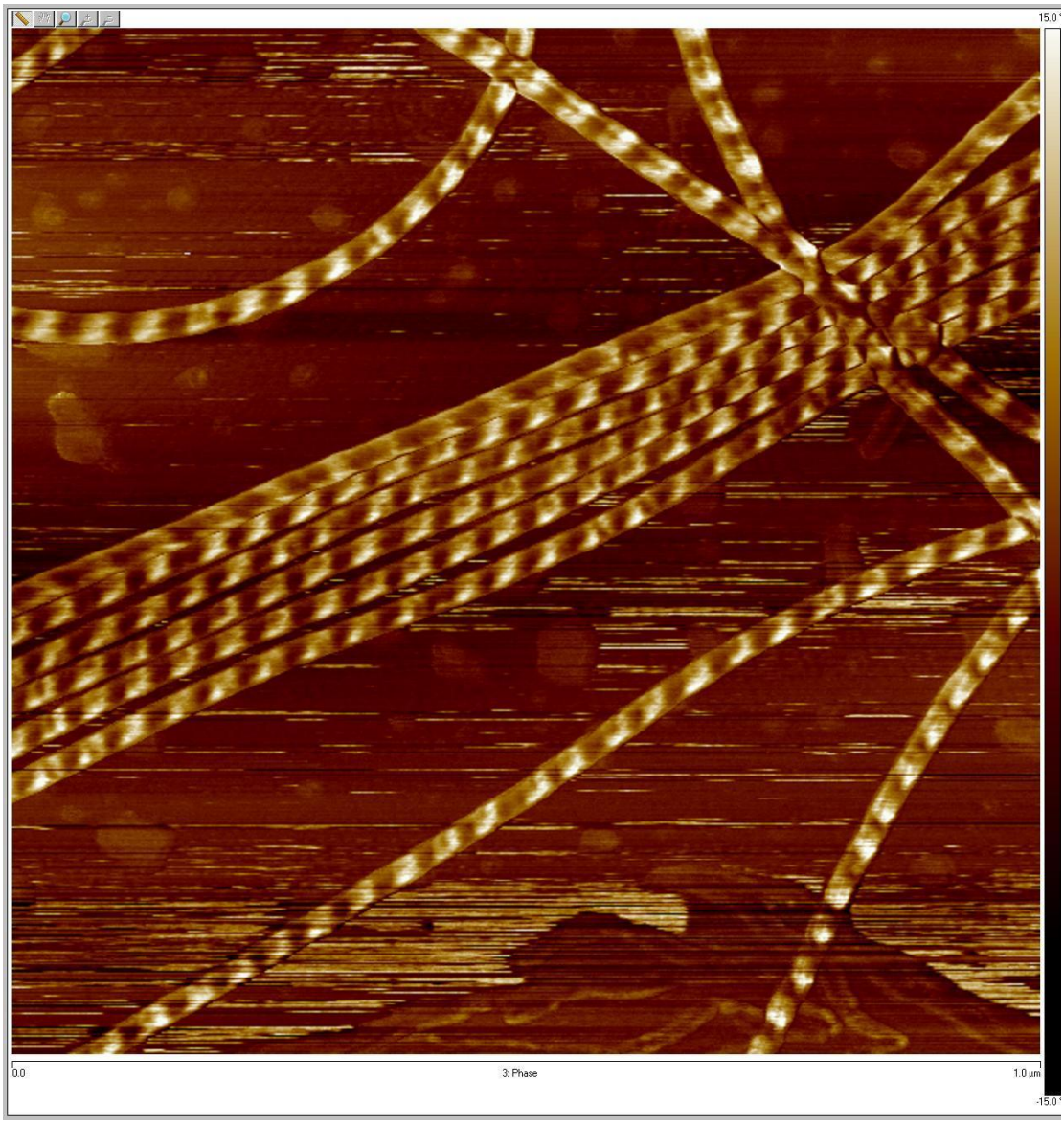

Figure S29. AFM phase image of sample (*S*)-**1** prepared by spin-coating of solution obtained by dilution of 0.127 wt-% chiral gels in acetonitrile to 0.025 wt-%.

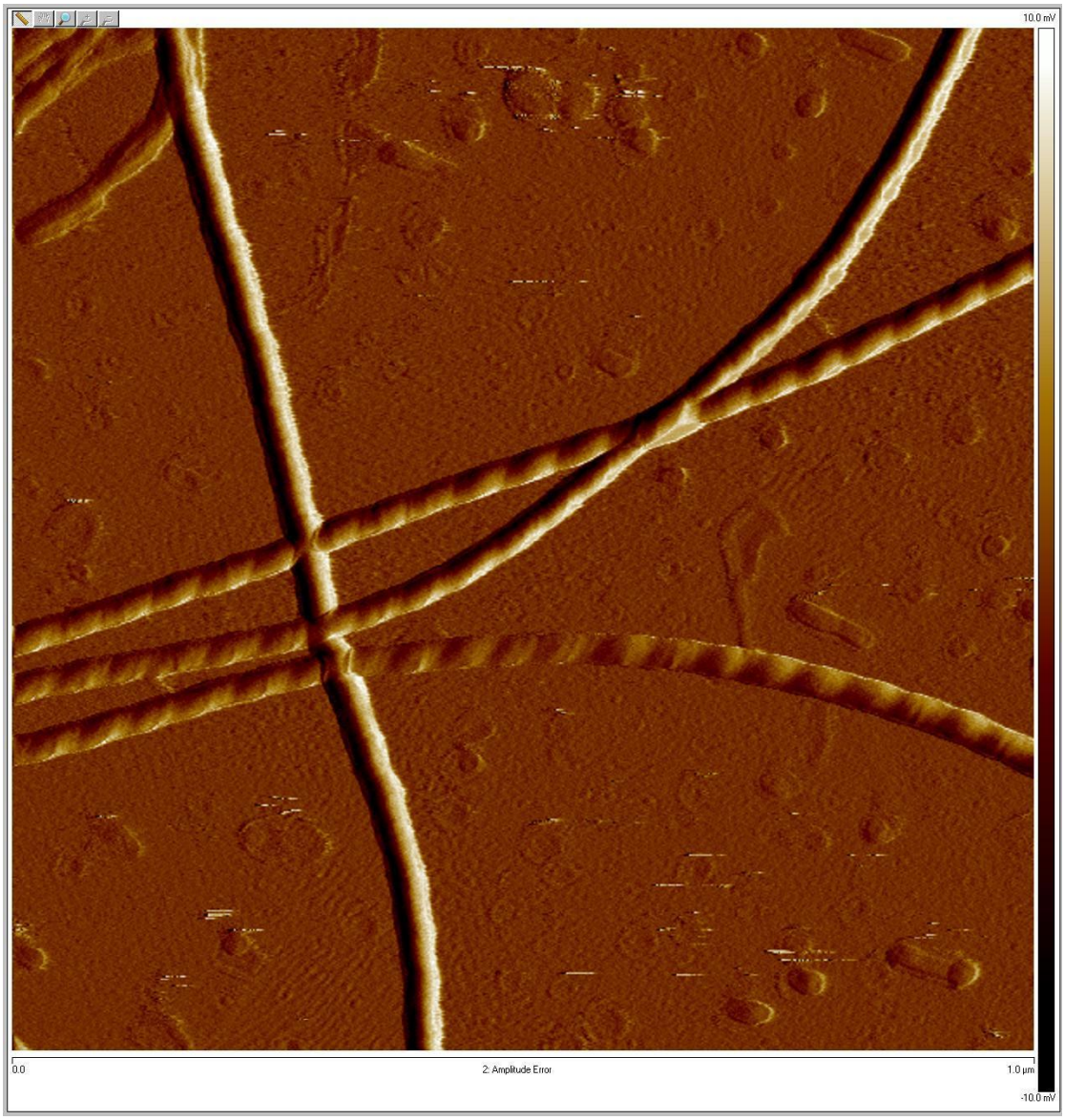

Figure S30. AFM amplitude error image of sample (*S*)-**1** prepared by spin-coating of solution obtained by dilution of 0.127 wt-% chiral gels in acetonitrile to 0.025 wt-%.

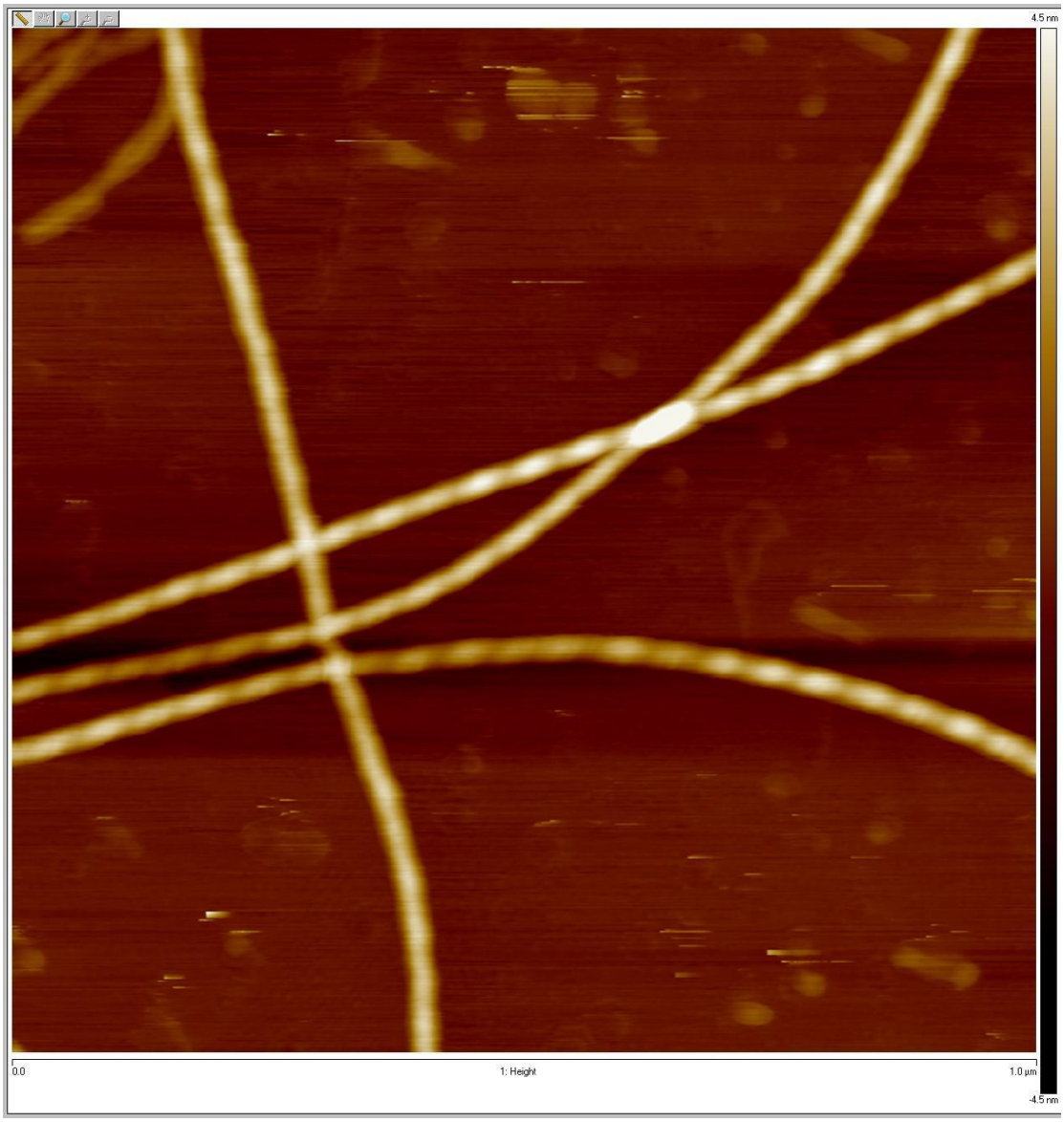

Figure S31. AFM height image of sample (*S*)-**1** prepared by spin-coating of solution obtained by dilution of 0.127 wt-% chiral gels in acetonitrile to 0.025 wt-%.

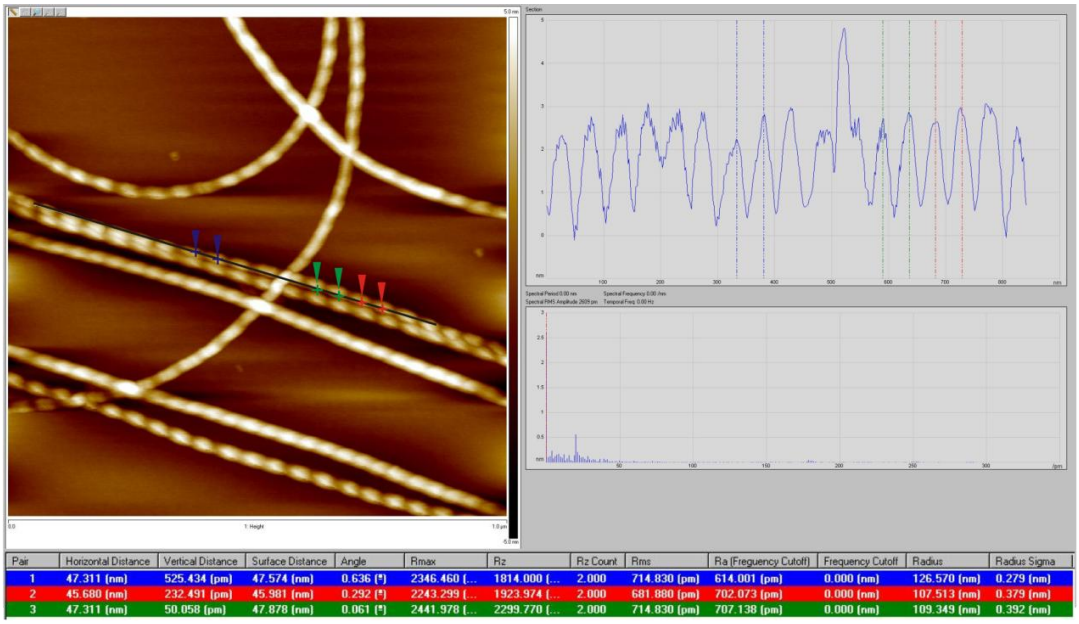

Pair	Horizontal Distance	Vertical Distance	Surface Distance	Angle	Rmax	Rz	Rz Count	Rms	Ra (Frequency Cutoff)	Frequency Cutoff	Radius	Radius Sigma
1	47.311 (nm)	525.434 (pm)	47.574 (nm)	0.636 (°)	2346.460 (...	1814.000 (...	2.000	714.830 (pm)	614.001 (pm)	0.000 (nm)	126.570 (nm)	0.279 (nm)
2	45.680 (nm)	232.491 (pm)	45.981 (nm)	0.292 (°)	2243.299 (...	1923.974 (...	2.000	681.880 (pm)	702.073 (pm)	0.000 (nm)	107.513 (nm)	0.379 (nm)
3	47.311 (nm)	50.058 (pm)	47.878 (nm)	0.061 (°)	2441.978 (...	2299.770 (...	2.000	714.830 (pm)	707.138 (pm)	0.000 (nm)	109.349 (nm)	0.392 (nm)

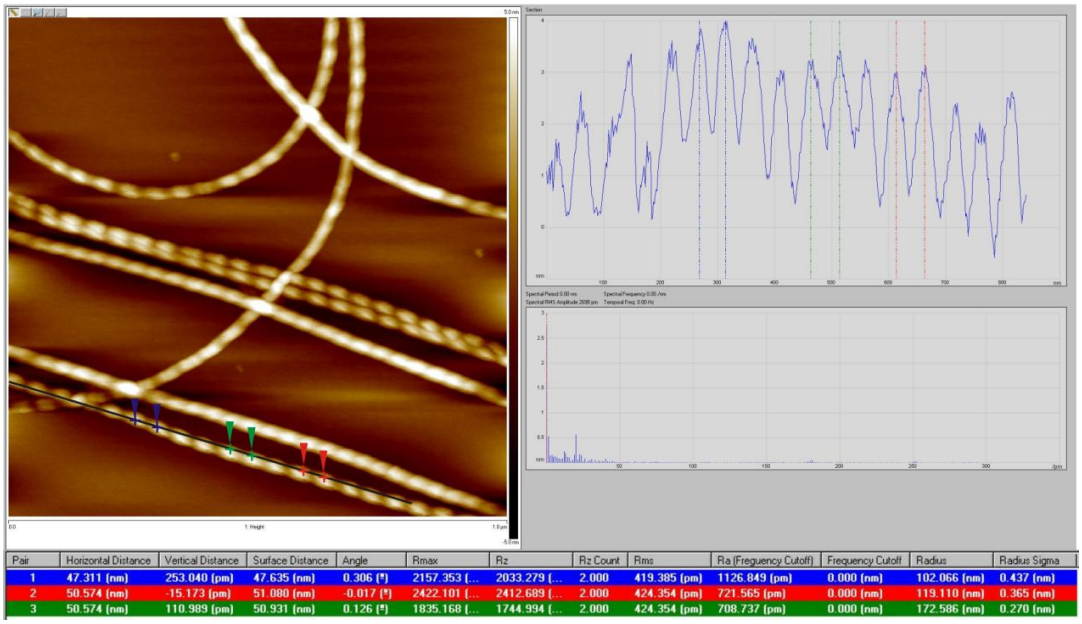

Pair	Horizontal Distance	Vertical Distance	Surface Distance	Angle	Rmax	Rz	Rz Count	Rms	Ra (Frequency Cutoff)	Frequency Cutoff	Radius	Radius Sigma
1	47.311 (nm)	253.040 (pm)	47.635 (nm)	0.306 (°)	2157.353 (...	2033.279 (...	2.000	419.385 (pm)	1126.849 (pm)	0.000 (nm)	102.066 (nm)	0.437 (nm)
2	50.574 (nm)	-15.173 (pm)	51.080 (nm)	-0.017 (°)	2422.101 (...	2412.689 (...	2.000	424.354 (pm)	721.565 (pm)	0.000 (nm)	119.110 (nm)	0.365 (nm)
3	50.574 (nm)	110.989 (pm)	50.931 (nm)	0.126 (°)	1835.168 (...	1744.994 (...	2.000	424.354 (pm)	708.737 (pm)	0.000 (nm)	172.586 (nm)	0.270 (nm)

Figure S32. Pitch analysis of chiral gelator (*R*)-**1**. The right-handed helical fibers exhibit a helical pitch of 48.0 ± 2.5 nm.

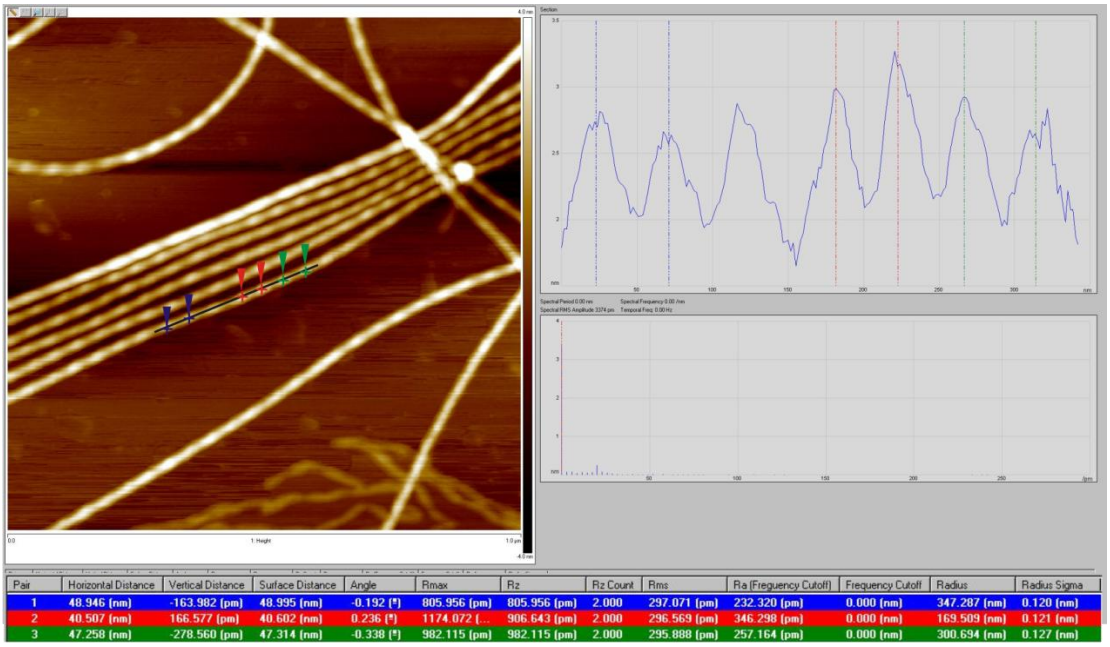

Pair	Horizontal Distance	Vertical Distance	Surface Distance	Angle	Rmax	Rz	Rz Count	Rms	Ra (Freguency Cutoff)	Frequency Cutoff	Radius	Radius Sigma
1	48.946 (nm)	-163.982 (pm)	48.995 (nm)	-0.192 (°)	805.956 (pm)	805.956 (pm)	2.000	297.071 (pm)	232.320 (pm)	0.000 (nm)	347.287 (nm)	0.120 (nm)
2	40.507 (nm)	166.577 (pm)	40.602 (nm)	0.236 (°)	1174.072 (...	906.643 (pm)	2.000	296.569 (pm)	346.298 (pm)	0.000 (nm)	169.509 (nm)	0.121 (nm)
3	47.258 (nm)	-278.560 (pm)	47.314 (nm)	-0.338 (°)	982.115 (pm)	982.115 (pm)	2.000	295.888 (pm)	257.164 (pm)	0.000 (nm)	300.694 (nm)	0.127 (nm)

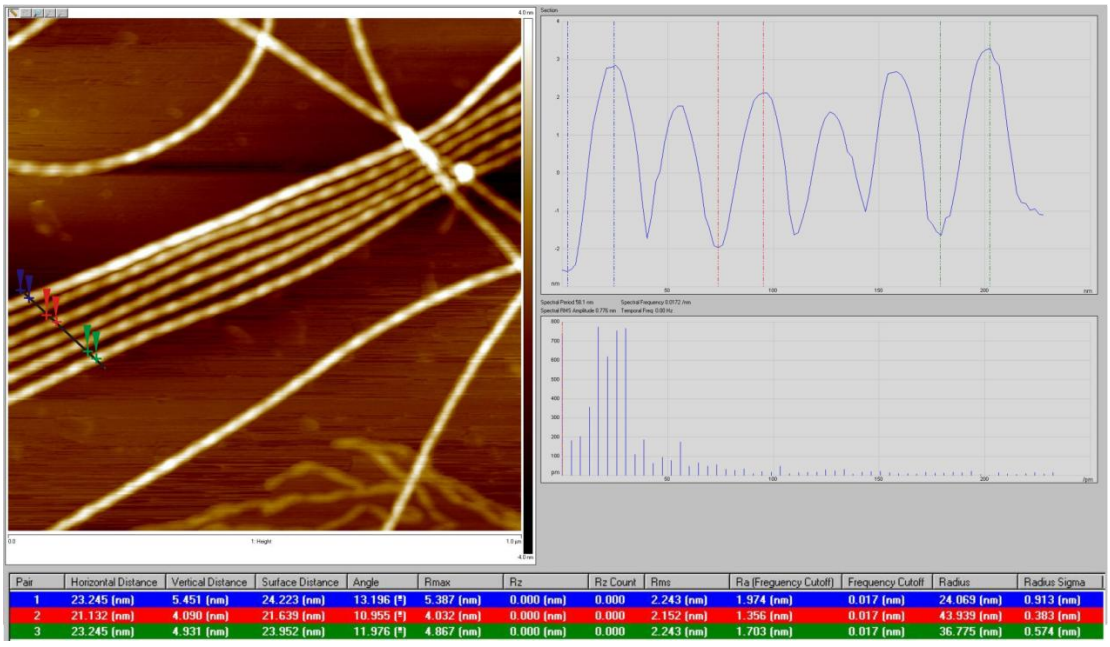

Pair	Horizontal Distance	Vertical Distance	Surface Distance	Angle	Rmax	Rz	Rz Count	Rms	Ra (Freguency Cutoff)	Frequency Cutoff	Radius	Radius Sigma
1	23.245 (nm)	5.451 (nm)	24.223 (nm)	13.196 (°)	5.387 (nm)	0.000 (nm)	0.000	2.243 (nm)	1.974 (nm)	0.017 (nm)	24.069 (nm)	0.913 (nm)
2	21.132 (nm)	4.090 (nm)	21.639 (nm)	10.955 (°)	4.032 (nm)	0.000 (nm)	0.000	2.152 (nm)	1.356 (nm)	0.017 (nm)	43.939 (nm)	0.383 (nm)
3	23.245 (nm)	4.931 (nm)	23.952 (nm)	11.976 (°)	4.867 (nm)	0.000 (nm)	0.000	2.243 (nm)	1.703 (nm)	0.017 (nm)	36.775 (nm)	0.574 (nm)

Figure S33. Pitch analysis of chiral gelator (*S*)-**1**. The left-handed helical fibers exhibit a helical pitch of 44.7 ± 4.2 nm.

4.8. Comparison of ^{1}H NMR Spectra of (R)-1 in Different Solvents

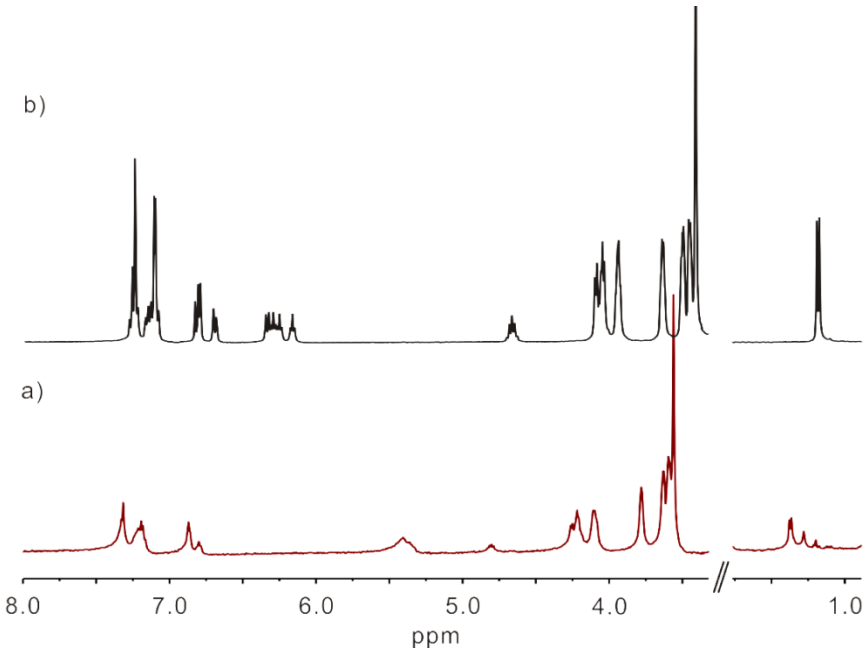

Figure S34. Partial ^{1}H NMR spectra (500 MHz, 293 K) of 5 mM solutions of (*R*)-**1** a) in CD_3CN where aggregation occurs and b) in DMSO-d_6 where the gelator is dissolved in monomeric form due to the higher donor strength of the solvent which disrupts the urea-urea hydrogen bonding

5. Characterization of the Stimuli-Responsiveness of the Supramolecular Gel

5.1. ^{1}H NMR Spectral Changes Observed upon KPF_6 Addition to (*R*)-1

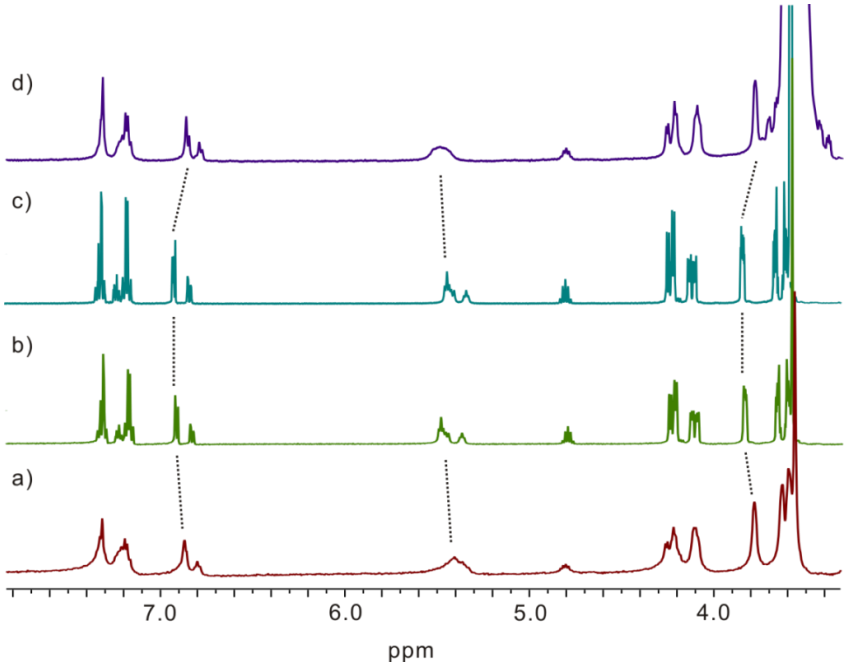

Figure S35. Partial ^{1}H NMR spectra (500 MHz, CD_3CN, 298K) of a) 5.0 mM (*R*)-**1**, b) the mixture obtained after adding 1.0 eq. KPF_6 to solution (a), c) the mixture obtained after adding 1.0 eq. KPF_6 to solution b), d) the mixture obtained after adding 4.0 eq. of [2.2.2]cryptand to solution c).

5.2. Control Experiment Excluding PF_6^- as the Trigger for the Gel-Sol Transition

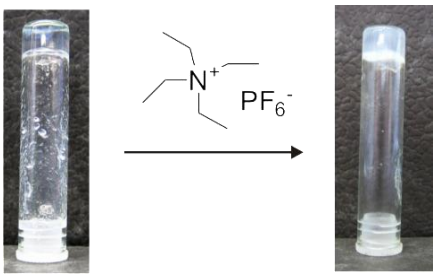

Figure S36. Photographs of the gelator (*R*)-**1** (20.8 mM in CD_3CN) and the mixture obtained after adding 2.0 eq. tetraethylammonium hexafluorophosphate (NEt_4PF_6). The retained gel phase indicates the PF_6^- anion not to trigger the gel-sol transition.

5.3. ^{1}H NMR Spectral Changes upon Addition of Monovalent Guest G1 to (*R*)-1

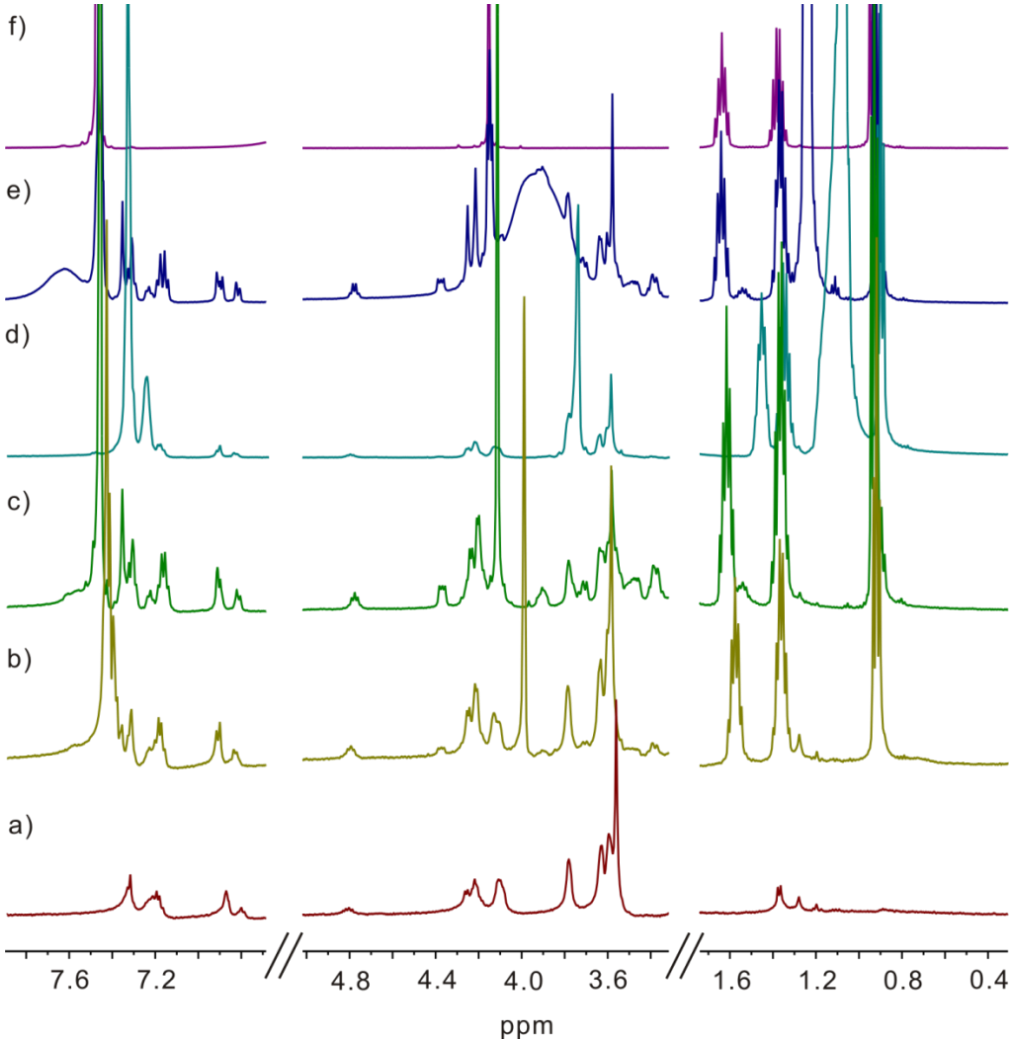

Figure S37. Partial ^{1}H NMR spectra (500 MHz, CD_3CN, 298 K): a) Compound (*R*)-**1** (5.0 mM) in its gel state. b) Spectrum obtained after adding **G1** (1.0 eq.) to solution a). c) after adding **G1** (2.0 eq.) to solution b). d) after addition of base (2.2 eq. TEA) to solution c). e) after addition of acid (2.0 eq. TFA) to solution d). f) Free **G1**.

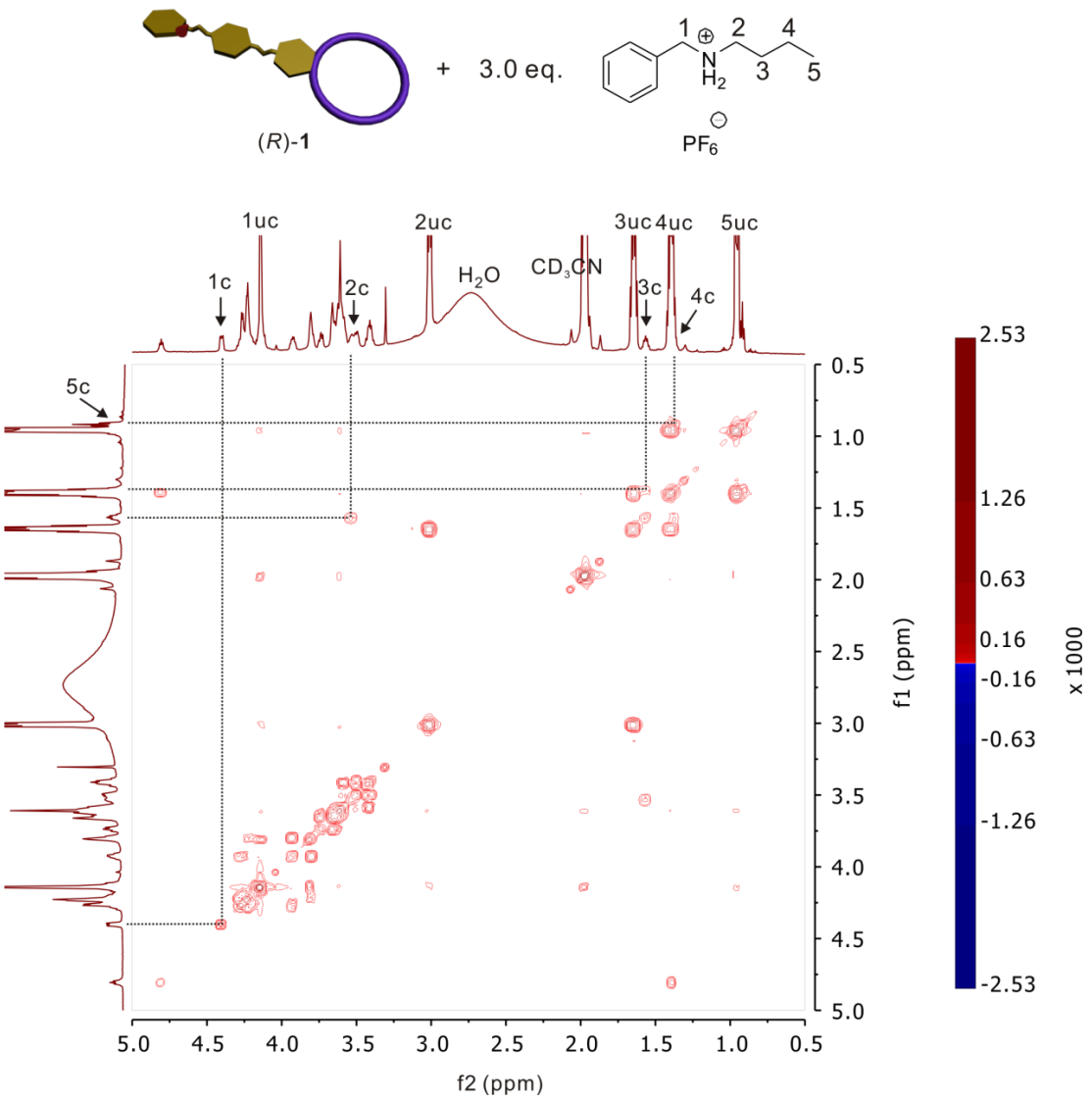

Figure S38. ^{1}H-^{1}H COSY NMR spectrum (500 MHz, 298 K, CD_3CN, 5.0 mM) of the 1:3 mixture of (*R*)-**1** and **G1**. The protons are labeled with the number indicated above plus "c" for complexed" and "uc" for uncomplexed"

5.4. Control Experiment Revealing Pseudorotaxane Formation as the Trigger for the Gel-Sol Transition

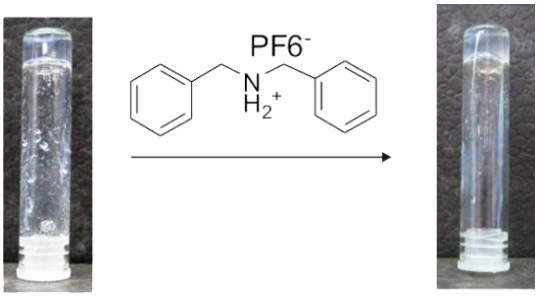

Figure S39. Photographs of gelator (*R*)-**1** (5.0 mM in CH_3CN) and the mixture obtained after adding 3.0 eq. of dibenzyl ammonium hexafluorophosphate. In contrast to G1, no gel-sol transition is induced. Since the phenyl groups of the dibenzyl ammonium ions are too large to penetrate the crown ether, no pseudorotaxane forms and the gel persists. This control experiment not only demonstrates again that the PF_6^- counterion does not interfere with gel formation. It also clearly shows that pseudorotaxane formation is the reason for the gel-sol transition, when **G1** is added.

5.5. ^{1}H NMR Changes upon NEt_4Cl Addition to (*R*)-1

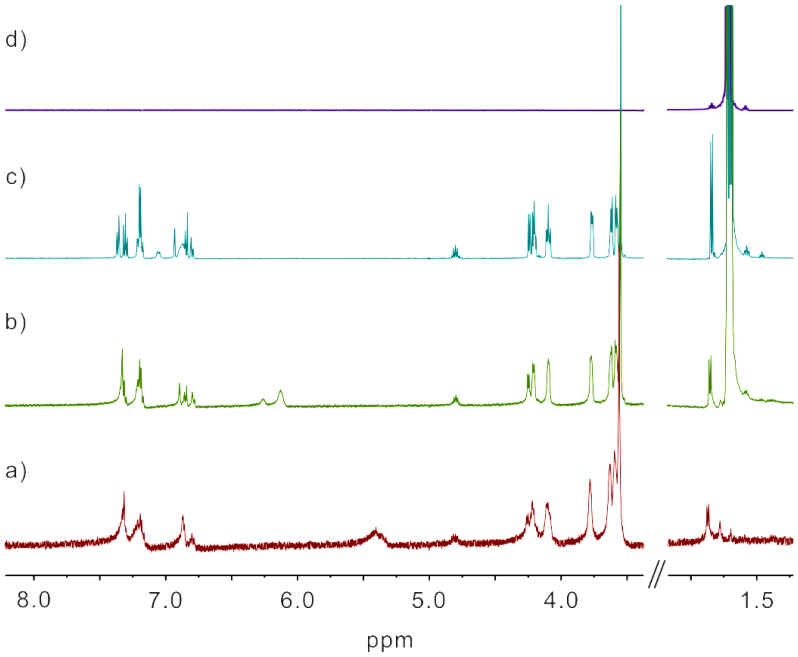

Figure S40 Partial ^{1}H NMR spectra (500 MHz, CD_3CN, 298K) of a) 5.0 mM (*R*)-**1**, b) the mixture obtained after adding 2.0 eq. NEt_4Cl to solution a), c) the mixture obtained after adding 6.0 eq. NEt_4Cl to solution b), d) 5 mM NEt_4Cl.

5.6. UV/Vis Experiments with Added Guests

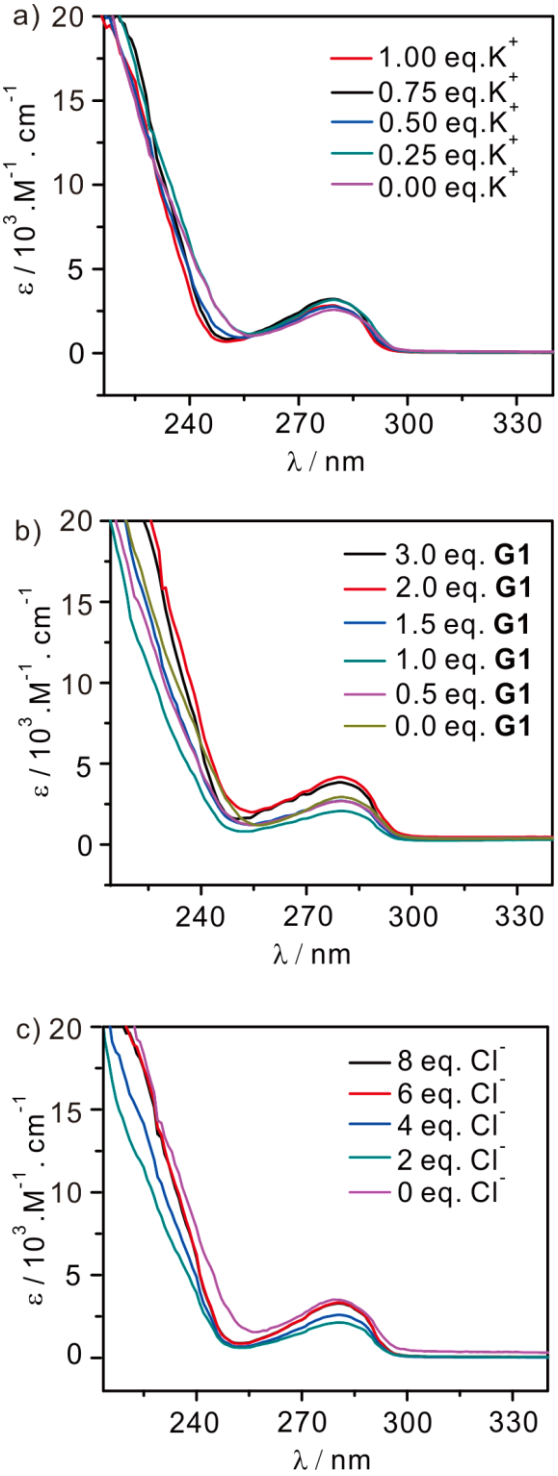

Figure S41. UV/Vis spectra of chiral gelator: (a) up to 1.00 eq. K^+ was added into (*R*)-**1** in acetonitrile; (b) up to 3.0 eq. monovalent axle **G1** was added into (*R*)-**1** in acetonitrile; (c) up to 8.0 eq. Cl- add into (*R*)-**1** in acetonitrile.

5.7. AFM and CD Investigation of Guest Recognition

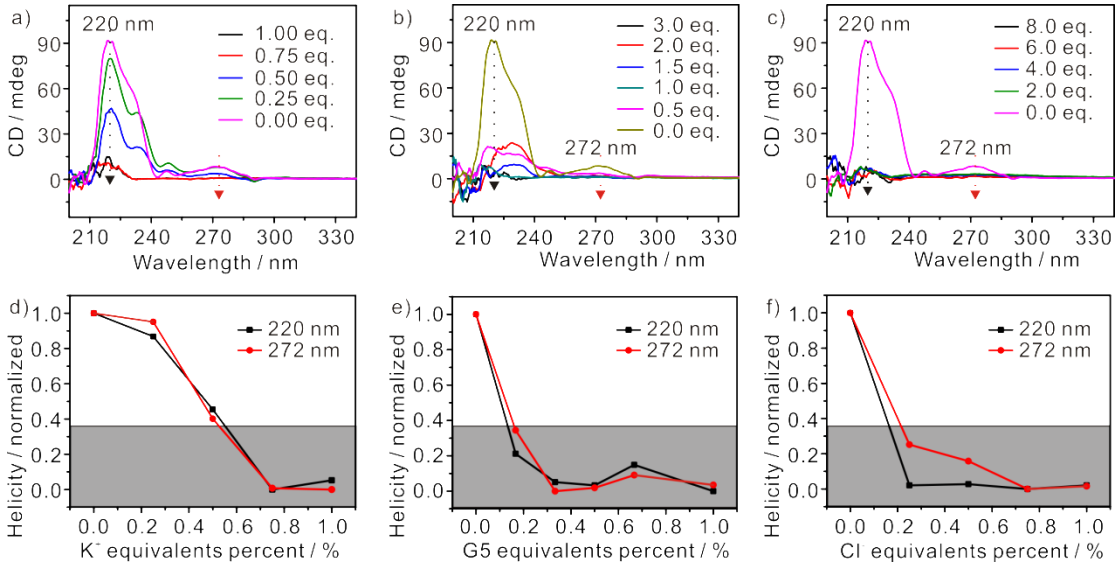

Figure S42. CD spectra of chiral gel (*R*)-**1** in acetonitrile with various guest: (*R*)-**1** (0.127 wt.-%) in its gel state as well as the spectra obtained a) after adding KPF_6 (0.25 - 1.0 eq.); b) after adding monovalent guest **G1** (0.5 - 3.0 eq.); c) after adding NEt_4Cl (2.0 - 8.0 eq.). d) - f) plots of the CD changes at 220 and 272 nm depending on the amount of the guest. The decrease of the CD signals with increasing amount of guest added shows them to destroy the gel as observed in the spectra a) - c), respectively. The grey boxes in Figure d-e are draw to compare the CD decline trend. These experiments again confirm the CD signals at 220 and 272 nm to reflect helix formation, while the monomers are CD silent.

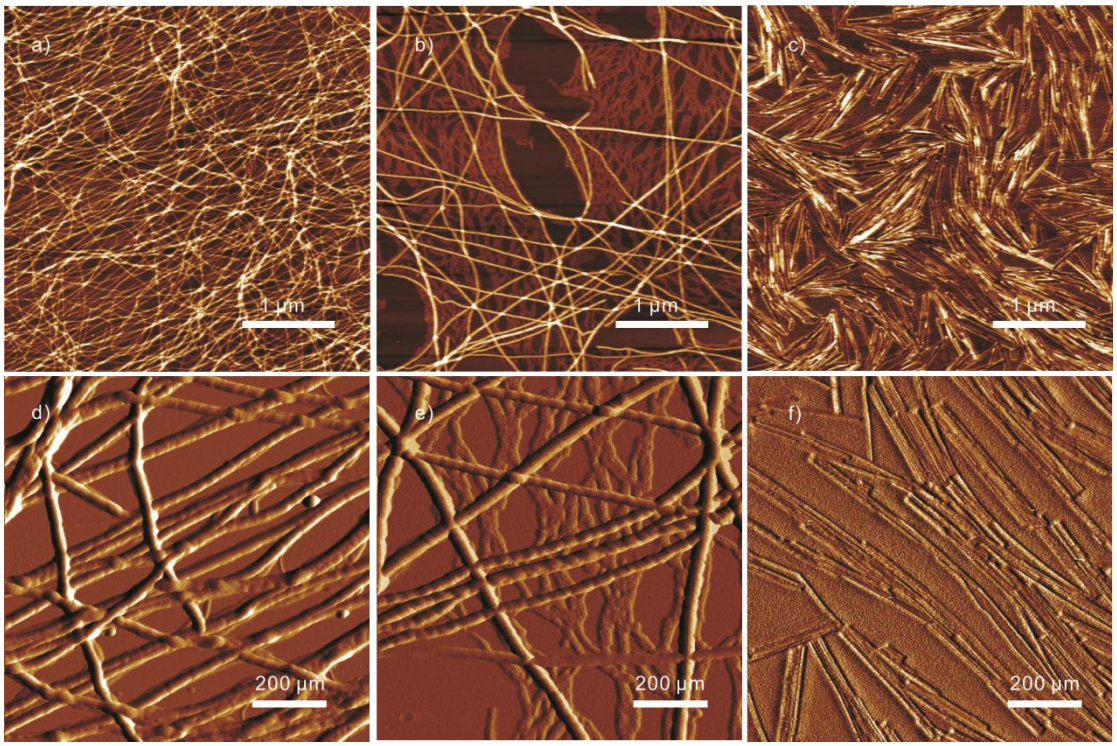

Figure S43. Morphology change induced by guest addition: AFM height (a-c) and amplitude error (d-f) images of chiral gelator (*R*)-**1** with different additives: (*R*)-**1** + 1.0 eq. KPF_6 (a, d); (*R*)-**1** + 0.5 eq. **G1** (b, e); (*R*)-**1** + 2.0 eq. NEt_4Cl (c, f).

5.8. AFM Investigation of the Reverse Sol-Gel Transition

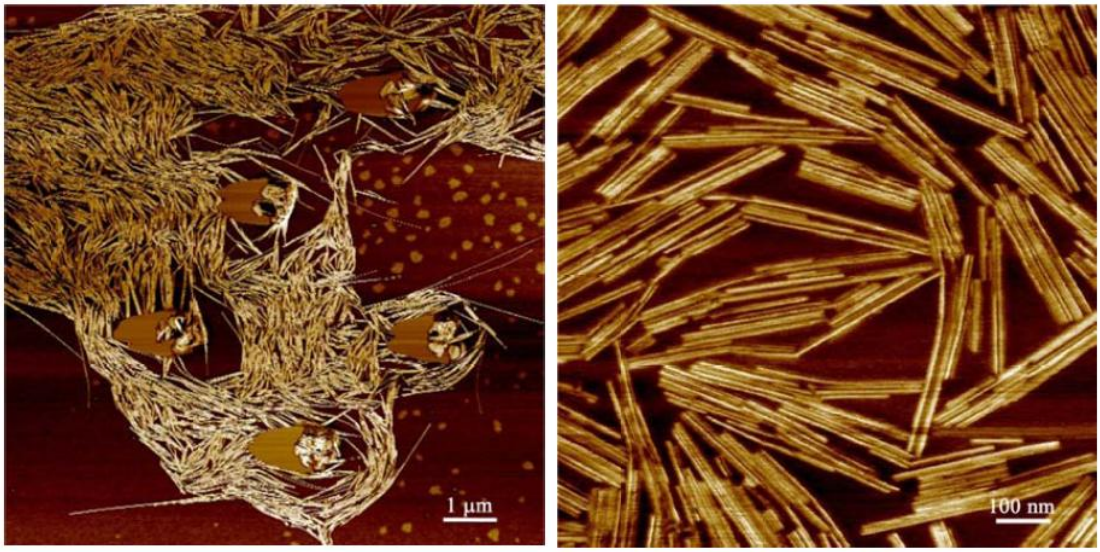

Figure S44. AFM phase images of (*R*)-**1** (0.127 wt-%) with 1.0 eq. K^+ and 2.0 eq. [2.2.2]cryptand.

6. Amplitude Sweep Experiment for the Supramolecular Gel

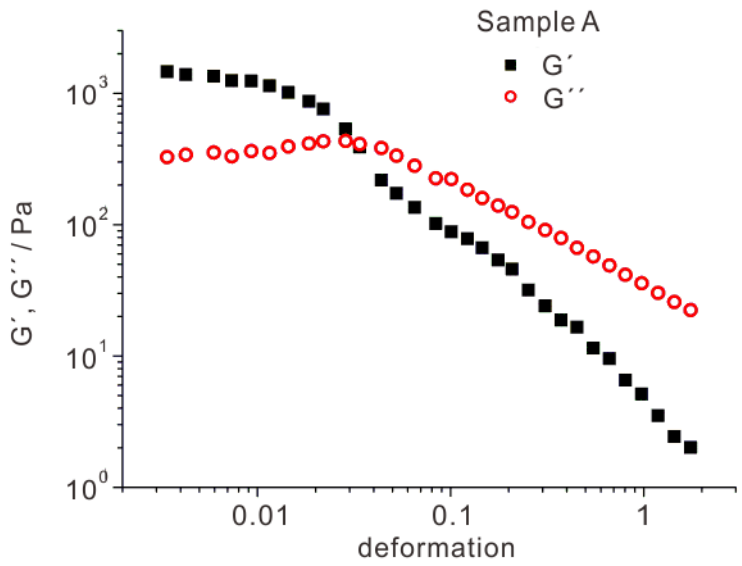

Figure S45. Oscillatory amplitude sweep of G' (filled squares) and G'' (open circles) of supramolecular gel (*R*)-**1** at an applied frequency of 1 Hz and a temperature of 25°C.

An amplitude sweep of the supramolecular gel (*R*)-**1** in acetonitrile (sample A in Figure 3 of maintext) was performed in order to determine the linear viscoelastic regime. Therefore, a fixed deformation of 0.01 was employed for all the gel samples. Additionally, the linear viscoelastic regime was ascertained by confirming the sinusoidal shape of the response function during the measurements.

7. Immobilization and Controlled Release of FITC-CalB from the Supramolecular Gel

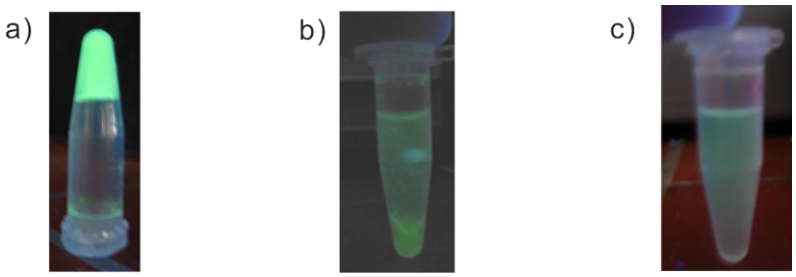

Figure S46. The photographs show a) the supramolecular gel of (*R*)-**1** loaded with FITC-CalB. This Figure shows the fibrous networks in the supramoelcular gel to trap the CalB in its gel matrix. b) Release of FITC-CalB when KPF_6 in water is added to the jellified emulsion droplets. c) Release of FITC-CalB when the jellified emulsion droplets are added to an excess of KPF_6 in acetonitrile. The whole phase becomes fluorescent indicating the full release of the enzyme. Figures S41b and S41c show the responsiveness of the gel and related to it the controlled release of the enzyme. Here the chemical trigger is K^+.

8. Reference

1. W. Stöber, A. Fink, E. Bohn, *J. Colloid Interface Sci.* **1968**, *26*, 62-69.